Environmentally regulated clonal-aggregative multicellularity in a choanoflagellate

Núria Ros-Rocher[1*], Josean Reyes-Rivera[2,3*], Uzuki Horo[1], Chantal Combredet[1], Yeganeh Foroughijabbari[1], Ben T. Larson[2,4], Maxwell C. Coyle[2,5], Erik A.T. Houtepen[6], Mark J. A. Vermeij[6,7], Jacob L. Steenwyk[2], Thibaut Brunet[1]

[1]Institut Pasteur, Université Paris-Cité, CNRS UMR3691, Evolutionary Cell Biology and Evolution of Morphogenesis Unit, 25-28 Rue du Dr. Roux, 75015 Paris, France

[2]Howard Hughes Medical Institute and the Department of Molecular and Cell Biology, University of California, Berkeley, Berkeley, CA, USA

[3]Present address: Department of Biochemistry and Biophysics, University of California, San Francisco, San Francisco, CA, USA

[4]Present address: Department of Biological Sciences and Center for Biotechnology and Interdisciplinary Studies, Rensselaer Polytechnic Institute, 110 8th St, Troy, NY, 12180, USA

[5]Present address: Department of Molecular and Cellular Biology, Harvard University, Cambridge, MA, USA

[6]Caribbean Research and Management of Biodiversity foundation (CARMABI), Piscaderabaai z/n Willemstad, Curaçao

[7]Department of Freshwater and Marine Ecology, Institute for Biodiversity and Ecosystem Dynamics, University of Amsterdam, Amsterdam, 1012 WP, The Netherlands

*Contributed equally

Correspondence: N. R.-R.: nuria.ros@pasteur.fr J. R.-R.: josean.reyesrivera@ucsf.edu T.B.: thibaut.brunet@pasteur.fr

Multicellularity evolved multiple times independently during eukaryotic diversification[1–4]. Two distinct mechanisms underpin multicellularity[5]: clonality (serial cell division without sister-cell separation) and aggregation (whereby independent cells assemble into a multicellular entity). Clonal and aggregative multicellularity are traditionally considered mutually exclusive[1,6–9], with rare exceptions[10], and evolutionary hypotheses have addressed why multicellularity might diverge toward one or the other extreme[3,4]. Both animals and their sister group, the choanoflagellates, are currently only known to acquire multicellularity clonally[4,11–13]. Here, we show that the choanoflagellate *Choanoeca flexa*[14] forms motile and contractile cell monolayers (or "sheets") through multiple mechanisms: *C. flexa* sheets can form purely clonally, purely aggregatively, or by a combination of both processes. We characterise the life history of *C. flexa* in its natural environment – ephemeral splash pools on the island of Curaçao – and show that *C. flexa* undergoes reversible transitions between unicellularity and multicellularity during cycles of evaporation and refilling. Different splash pools house genetically distinct strains of *C. flexa,* between which aggregation is constrained by kin recognition[15–18]. We show that clonal-aggregative multicellularity serves as a versatile strategy for the robust re-establishment of multicellularity in this variable and fast-fluctuating environment. Our findings challenge former generalisations about choanoflagellates and expand the option space of choanozoan multicellularity.

Multicellularity has evolved independently more than 45 times across eukaryotes[19], with multiple independent origins of both clonal and aggregative multicellularity[7,20]. Efforts to reconstruct the origin of animal multicellularity have benefited from the study of their closest living relatives, the choanoflagellates (**Figure 1A**)[21–24]. Choanoflagellates are bacterivorous aquatic microeukaryotes bearing an apical flagellum surrounded by a collar of actin-filled microvilli (**Figure 1B-C**)[25]. Moreover, many choanoflagellate species display facultative multicellularity[25]. The best-characterised choanoflagellate, *Salpingoeca rosetta*, forms colonies exclusively clonally[26], and clonal multicellularity has classically been assumed to be a general feature of choanoflagellates[4,25,27]. However, this assumption remains to be tested across choanoflagellate diversity. Interestingly, while animal multicellularity is purely clonal, other close relatives of animals besides choanoflagellates exhibit diverse forms of multicellularity, including aggregation in filastereans[28–31] as well as cellularization of multinucleated cells[32,33] and cleavage-like serial cell divisions in ichthyosporeans[33–36].

Here, we describe an unusual mode of multicellularity in the choanoflagellate *Choanoeca flexa*[14] that challenges prevailing assumptions about choanoflagellates. We show that *C. flexa* colonies can form by serial cell division, aggregation, or a combination of both, a mechanism we refer to as 'clonal-aggregative multicellularity'. We propose that this mode of multicellularity represents an adaptation to the dynamic natural environment of *C. flexa*: ephemeral splash pools that undergo extreme salinity fluctuations during natural cycles of evaporation and refilling.

C. flexa sheets can form clonally

C. flexa was discovered in 2018 in the form of curved monolayers of polarised cells (or 'sheet colonies') held together through direct collar-collar adhesions[14] (**Figure 1A-D**). *C. flexa* sheets can reversibly invert their curvature in response to light-to-dark transitions, switching between a feeding state (relaxed form, flagella-in; **Figure 1B**) and a swimming state (inverted form, flagella-out; **Figure 1D**)[37,38]. In an earlier study, we established stable cultures of *C. flexa* sheets from a single isolated cell, indicating that sheets can arise from individual cells[37]. Nevertheless, the mechanisms that establish multicellularity in *C. flexa* remain unknown.

To understand *C. flexa* colony formation, we isolated and monitored single cells from mechanically disassembled sheets by time-lapse microscopy. In this context, we observed clonal formation of sheets by serial cell division of single cells (**Figure 1E-F; movie S1**): cells divided asynchronously every ~8-10 hours, and sister cells remained attached to each other by collar-collar contacts. This resulted in a monolayer of polarised cells with the signature curved morphology of *C. flexa* sheets (**Figure 1B,E; movie S1**). These observations show that small *C. flexa* sheets (up to 7 cells) can form clonally. To test whether clonality can contribute to the further growth of *C. flexa* colonies, we monitored small and medium-sized colonies (from 6 to 46 cells) by time-lapse microscopy and observed clonal expansion by cell division both at the core and the periphery of the sheets (**Figures 1G** and **S1; movies S2-S3**). However, and unexpectedly, we also captured instances of free-swimming single cells and doublets meeting colonies, attaching to their periphery, reorienting to align their main apico-basal polarity axis with neighbouring cells, and seemingly integrating into the sheet (**Figures 1G** and **S1; movies S2-S3**). These results suggested that *C. flexa* colonies could form clonally but might also expand by aggregation. This motivated us to test whether *C. flexa* might be capable of purely aggregative multicellularity (**Figure 1H**).

C. flexa sheets can form by aggregation

To test whether *C. flexa* colonies can form by aggregation, we mechanically disassembled colonies into free-swimming single cells and performed live imaging of the dissociated cells (**Figure 2A-D; movies S4-S6**). Surprisingly, *C. flexa* single cells aggregated within minutes into cell doublets connected by collar-collar contacts (**Figure 2C; movie S5**). Doublets grew into larger groups of cells both through the incorporation of additional solitary cells and through fusion between groups (**Figure 2D; movie S6**). Early aggregates were often irregular in shape, reflecting initial collision and adhesion in diverse, random orientations. Aggregates later underwent morphological maturation through cellular rearrangements and reorientation into polarised monolayers with canonical *C. flexa* sheet morphology (**Figure 2D; movie S6**).

To quantify the dynamics of aggregation and maturation, we fixed sheets at successive stages of aggregation, followed by membrane and F-actin staining and Airyscan confocal imaging (**Figures 2E-G** and **S2; movies S7-S11**). We quantified two morphological metrics: the adhesion angle between the collars of neighbouring cells (or collar-collar angle) and the proportion of cells with aligned apico-basal polarity (**Figures 2F** and **S2A**). Both metrics initially showed high variance, consistent with variable cell orientations at early stages, and progressively converged towards stereotypical values during maturation (**Figures 2E-G** and **S2; movies S7-S11**). Moreover, early aggregates showed diverse types of intercellular contacts, including collar-collar, collar-cell body, and cell body-cell body contacts (**Figures 2E** and **S2B**). By contrast, mature colonies resulting from 24 hours of aggregation were polarised monolayers of cells connected almost exclusively by collar-collar contacts (**Figures 2E** and **S2B; movie S11**). At that stage, colonies comprised about 50 cells on average and up to 120 cells (**Figures 2G''** and **S2D**). This size further confirmed that they could not have formed exclusively through cell division within 24 hours, given the cell cycle duration in *C. flexa* (at least 8 hours; **Figure 1F**), which would allow for sheets of at most 16 cells, assuming maximal and synchronised proliferation.

To independently confirm that the regular sheets observed 24 hours post-dissociation (hpd) resulted from the maturation of early aggregates, we performed aggregation assays by mixing two populations of dissociated single cells stained with different fluorophores (**Figures 2H** and **S3; movies S12-S13**). Cells of both colours assembled within minutes into irregular chimeric aggregates (**Figure S3A; movie S12**). After 24 hours, we observed chimeric polarised monolayers composed of cells of both colours (**Figures 2H** and **S3B-C; movie S13**),

132 confirming their aggregative origin. Furthermore, treatment with the cell cycle inhibitor
133 aphidicolin did not abolish aggregation (**Figure 2I** and **S4**), confirming that aggregation can
134 occur independently of cell division. Finally, we sought to determine whether aggregation was
135 an active process or whether it might simply result, at least at early stages, from passive cell
136 stickiness. While live cells readily aggregated, fixed cells did not (even under orbital agitation
137 forcing cell encounters), suggesting that aggregation requires live cells and is thus an active
138 process (**Figure S5**).
139 Taken together, these data indicate that *C. flexa* sheets can form by aggregation. This
140 process is independent of cell division, is active, and occurs in multiple steps: random cell
141 collisions initially form irregular clumps of variable morphology, which then mature into regular,
142 polarised monolayers of cells via cell reorientation.
143 The discovery of clonal-aggregative multicellularity in *C. flexa* contrasts with prevailing
144 assumptions about choanoflagellates, which – based largely on studies of the model species
145 *S. rosetta*[39] – were thought to acquire multicellularity only clonally. Notably, clonal and
146 aggregative multicellularity usually occupy different ecological niches: aggregation is often an
147 'emergency response' to sudden stress[3,40], whereas clonality requires sufficiently stable
148 environmental conditions to sustain cell division. This prompted us to investigate the natural
149 environmental context in which *C. flexa* might employ clonal-aggregative multicellularity.
150

151 **Occurrence of multicellular *C. flexa* in the field is limited by salinity**

152

153 *C. flexa* was originally discovered in its multicellular form on the tropical island of
154 Curaçao[14] (**Figure 3A**). Unlike other multicellular choanoflagellates[22,41], *C. flexa* has been
155 repeatedly re-isolated in the field since its discovery in 2018 and can thus be studied in its
156 native biotope. *C. flexa* sheets are found on the windward, northern part of the island, in splash
157 pools that undergo natural cycles of evaporation and refilling[42,43] (**Figures 3A-C** and **S6A-B;**
158 **movie S14**). Water-filled splash pools gradually evaporate, leading to increasing salinity and,
159 occasionally, complete desiccation (**Figure 3C**). Splash pools are subsequently refilled by
160 waves, splash, or rain, restoring lower salinity levels (**Figures 3C** and **S6B; movie S14**). As
161 a consequence, splash pools are ephemeral habitats in which organisms are exposed to
162 extreme and recurrent hypersaline and hyperosmotic stress[43–46]. We therefore set out to
163 investigate how this dynamic habitat might influence the life history and multicellularity of *C.*
164 *flexa*.

We focused our studies on Shete Boka National Park, where *C. flexa* is consistently found (**Figure 3A**). We measured salinity and scored the presence of *C. flexa* sheets in 150 splash pools in two different field expeditions, Exped-A and Exped-B (**Figures 3D** and **S6; Table S1**). During Exped-A, we sampled 79 splash pools (numbered Sp1 to Sp79) along approximately 2 kilometres of coastline (**Figure 3D**; see Materials and Methods for details). While seawater collected from adjacent inlets (or *bokas*) had a stable salinity of ~40 parts per thousand (ppt; **Table S1**), splash pool salinity ranged from below that of average seawater salinity (15 ppt) to saturation (≥ 280 ppt) (**Figures 3E** and **S6D; Table S1**). In 10 of the 79 splash pools, we found choanoflagellate sheets that we identified as *C. flexa* based on morphology, inversion behaviour, and 18S ribosomal DNA (rDNA) sequencing (**Figures 3F** and **S7; movie S15; Tables S1-S2; Supplementary files S1-S4**). *C. flexa* sheets were not observed in the other 69 splash pools. Interestingly, although the salinity of surveyed splash pools ranged from 15 to 280 ppt, *C. flexa* sheets were predominantly found in splash pools with ~2-fold seawater salinity during Exped-A (**Figures 3E** and **S6D; Table S1**). To independently test whether the presence of multicellular *C. flexa* was constrained by an upper salinity limit, we exhaustively sampled all splash pools within a 4-meter by 10-meter quadrant during a second expedition (Exped-B; n=71 splash pools, numbered M1 to M71; **Figure 3D'** and **S6C; Table S1**). We observed sheets in 14 splash pools and not in 57 others, with a maximum salinity threshold of 94 ppt for sheet occurrence (**Figures 3E** and **S6D**). Across both expeditions, *C. flexa* sheets were found in splash pools with an average salinity of 62.1±24.8 ppt (equivalent to 1.55-fold seawater salinity; **Figures 3E; Table S1**), which was significantly lower than the salinity of splash pools in which sheets were not observed (146.3±95.7 ppt; p=1.7e-06 by the Mann-Whitney U test; **Figures 3E; Table S1**). Across both expeditions, we never observed actively swimming and inverting *C. flexa* sheets in splash pools exceeding 128 ppt (~3-fold seawater salinity; **Figures 3E** and **S6D; Table S1**).

Natural evaporation-refilling cycles cause reversible transitions between unicellular and multicellular states in splash pools

We next examined how the natural evaporation-refilling cycles of splash pools impacts the occurrence of sheets. We monitored ten splash pools where *C. flexa* sheets had already been found during Exped-A, along with five additional randomly selected splash pools, once per day during eight days (**Figures 3E,G-H** and **S8**). We recorded salinity and maximum depth, and noted the presence of sheets (**Figures 3E,G-H** and **S8**). We observed a progressive

199 increase in salinity and decrease in depth in all 15 splash pools (presumably due to
200 evaporation; **Figure S8A-B**), with six desiccation events (**Figure S8C-D**) and four refilling
201 events (**Figure S8E-F**; three examples are shown in **Figure 3H**). In all cases, actively
202 swimming and inverting *C. flexa* sheets were no longer observed after salinity exceeded a
203 128 ppt threshold during gradual evaporation (**Figures 3H** and **S8**), consistent with results
204 from Exped-A and Exped-B (**Figures 3E-H** and **S8**). Interestingly, we observed two isolated
205 colonies with an apparently stressed phenotype (characterized by irregular outlines, loose cell
206 packing, lack of flagellar beating, and absence of inversion behaviour) at 200 and 212 ppt in
207 two different splash pools (Sp64 and Sp69, respectively on Days 4 and 3; **Figures 3H** and
208 **S8E-F; Table S1**). These irregular and inactive colonies were not observed at later time
209 points, suggesting they had either died or dissociated (**Figures 3H** and **S8F; Table S1**).
210 Similarly, gradual evaporation in the laboratory of a natural splash pool sample containing
211 sheets led to sheet disappearance (**Figure S9**). These observations confirmed that the
212 multicellular form of *C. flexa* does not tolerate high salinity.
213 Notably, in two dry splash pools that underwent refilling during our study (where salinity
214 was restored to ~50 ppt), sheets were observed 48 hours after refilling (Sp69 and Sp70;
215 **Figures 3H** and **S8E-F**). The newly observed sheets may have originated from the ocean or
216 from neighbouring splash pools. Alternatively, *C. flexa* might have persisted in the soil of
217 desiccated splash pools in a cryptic resistant form, such as unicellular cysts (as described in
218 other choanoflagellates[47–49]). To test this possibility *in situ*, we collected soil samples from six
219 desiccated splash pools in which *C. flexa* had been previously observed, rehydrated them in
220 the laboratory, and monitored the rehydrated samples for several days (**Figure 3I-K; movie**
221 **S16** and **Table S1**). Sheets were consistently recovered from soil samples from two splash
222 pools after 2-7 days of desiccation in the field followed by 2-3 days of rehydration in the
223 laboratory, suggesting that a resistant form of *C. flexa* can survive complete desiccation
224 (**Figure 3I-K** and **Table S1**).
225 Given that salinity fluctuations in splash pools seemed to impact *C. flexa* multicellularity in
226 nature, we next set out to investigate the phenotypic response of *C. flexa* to comparable
227 evaporation-refilling cycles in a laboratory context.
228
229 **Evaporation-refilling cycles cause reversible transitions between multicellular**
230 **and unicellular states in the laboratory**
231

232 To mimic natural evaporation-refilling cycles in the laboratory, we subjected *C. flexa*
233 cultures to gradual evaporation in an incubator (**Figure 4A**), replicating the temperature
234 (30°C) and evaporation rate of natural splash pools (**Figure 4B** and **S10A;** see Materials and
235 Methods). Starting from the standard salinity of artificial seawater (35 ppt; hereafter '1X
236 salinity'), this resulted in complete desiccation after four days. Under these conditions, *C. flexa*
237 sheets gradually dissociated into non-motile single cells (**Figures 4C-D** and **S10B; movie**
238 **S17**), with more than 50% solitary cells observed once salinity crossed the natural limit of
239 active sheet occurrence (128 ppt; **Figures 3E** and **4C-D**). By the time salinity reached
240 saturation, nearly all sheets had dissociated into single cells (**Figures 4C-D** and **S10B; movie**
241 **S17**). By contrast, control cultures maintained under constant conditions without evaporation
242 remained multicellular throughout the experiment (**Figure S10C**). Finally, to directly test
243 whether the loss of multicellularity was caused by increased salinity, we added seawater salt
244 to *C. flexa* cultures (without evaporation) and similarly observed dissociation of multicellular
245 sheets into single cells (**Figure S11A-C**).
246 We then tested whether single cells resulting from sheet dissociation were viable and
247 capable of surviving desiccation. We rehydrated samples by adding artificial seawater three
248 hours after desiccation, thereby mimicking refilling by waves. This restored salinity to ~50 ppt
249 and was followed by the reappearance of multicellular sheets within 24 hours post-
250 rehydration, as well as by a continuous increase in the number of colonies over the following
251 days (**Figure 4C-D**). We assessed the mechanism of colony re-formation by time-lapse
252 microscopy of desiccated cultures after rehydration and captured instances of unicellular
253 flagellates engaging in both clonal divisions and aggregation (**Figure S10D; movie S18**).
254 Taken together, our results show that *C. flexa* sheets dissociate into non-motile single
255 cells during gradual evaporation, that these solitary cells can survive complete desiccation,
256 and that sheets reform after rehydration through both clonal division and aggregation. These
257 findings are consistent with our field observations, where we recovered sheets after
258 rehydrating soil samples from dry splash pools (**Figure 3I-K** and **Table S1**), and further
259 support the existence of a desiccation-resistant form of *C. flexa*.
260

261 ## *C. flexa* sheets undergo dissociation-encystation at high salinity

262

263 We next investigated the phenotype of desiccation-induced single cells. In diverse protists,
264 resistance to desiccation is achieved through differentiation into cysts[50–52] – dormant cells
265 characterized by reduced metabolic activity and proliferation. Encystation often entails

266 significant morphological changes, including cell rounding, flagellar loss, and the formation of
267 a protective cell wall[47,50]. We monitored cellular morphology by DIC microscopy during gradual
268 evaporation and observed asynchronous structural changes that produced a heterogeneous
269 cell population (**Figure 4E-H**). At 3X salinity, most cells had dissociated from their colonies
270 and displayed a rounded cell body lacking microvilli, often missing a flagellum and
271 occasionally bearing filopodia-like protrusions (**Figure 4F-H**). Membrane and F-actin staining
272 of desiccation-resistant cells (hereafter 'cysts') confirmed the absence of a collar complex and
273 revealed a transient F-actin cortex, detectable at 3X salinity but lost above 6X (near saturation;
274 **Figures 4I-K** and **S12**). This cortex may help protect the plasma membrane against osmotic
275 stress during early differentiation[53–56]. Cysts did not proliferate: growth was arrested above 2X
276 salinity, with a net cell loss above 3X salinity (**Figures 4L** and **S13**), similar to cell cycle arrest
277 during encystation in other protists[50,57]. Finally, morphometric analysis of cell body and
278 nucleus volume showed that cysts had a larger nucleus-to-cytoplasm ratio compared with
279 flagellates at 1X salinity (**Figure S14**). An increase in the nucleus-to-cytoplasm ratio is
280 frequently associated with cell quiescence[58], consistent with growth arrest in *C. flexa* cysts.
281 To confirm that these changes were induced by hypersaline stress, we directly increased the
282 salinity of *C. flexa* cultures by adding seawater salts and observed similar morphological
283 changes and arrest in cell growth (**Figure S11**). Thus, the cellular changes induced by
284 hypersalinity in *C. flexa* closely resemble encystation in diverse other protists[50,59].
285 Sheet dissociation during encystation is likely caused by retraction of the microvilli that
286 connect neighbouring cells within colonies[14]. We tested this hypothesis by inducing microvillar
287 retraction (independently of encystation) by treatment with the actin-depolymerizing
288 compound latrunculin B, and observed dissociation of colonies within minutes (**Figure S15A-**
289 **D**). Similarly, latrunculin B treatment of single cells prevented aggregation (**Figure S15E-H**).
290 These results confirm that microvillar integrity is necessary for multicellularity in *C. flexa* and
291 further support the idea that sheets undergo a coupled dissociation-encystation process under
292 hypersaline conditions.
293 During the natural evaporation-refilling cycles of splash pools, *C. flexa* therefore alternates
294 between multicellular, flagellated sheets (at low salinity) and unicellular cysts (at high salinity),
295 suggesting these two phenotypes each confer an adaptive advantage in their respective
296 environments (**Figure 4M**). We then sought to directly test these putative advantages under
297 laboratory conditions.
298

Multicellular sheets and unicellular cysts are respectively advantaged at low and high salinity

If *C. flexa* cysts represent a desiccation-resistant form, we could expect these cells to be more resistant to hypersaline stress and desiccation than the sheets. To test this, we induced the differentiation of *C. flexa* sheets into cysts by gradual evaporation, following the protocol detailed in the previous section (from 1X salinity to complete desiccation over 72 hours). In parallel, we subjected sheets to rapid evaporation, causing desiccation over a period of 20 hours from 1X salinity (see Materials and Methods). Under these conditions, cells did not acquire a cyst-like morphology but instead retained their flagellum, collar, and multicellular morphology, even when completely desiccated (**Figure S16A**). This observation suggests that the formation of cysts requires gradual evaporation at a rate comparable to that of natural splash pools. After desiccation, we rehydrated both types of cells by adding artificial seawater and monitored their recovery. We found that desiccated sheets that had undergone rapid evaporation never gave rise to viable cells after rehydration (**Figure 4N**). In contrast, rehydrated cysts consistently gave rise to viable sheets (**Figure 4N**). These observations show that cysts, unlike flagellates, are equipped to survive hypersalinity and desiccation, and suggest that encystation confers a selective advantage during evaporation.

We further wondered whether multicellularity, by contrast, was advantageous in the other phase of the evaporation-refilling cycle, marked by low salinity. Multicellular choanoflagellates have been proposed to feed more efficiently, thanks to cooperative hydrodynamic interactions between flagella that enhance prey capture[60–62], although attempts to test this hypothesis in *S. rosetta* have yielded conflicting results[60,63,64]. To test for a feeding advantage in multicellular *C. flexa* sheets, we quantified the capture of fluorescent bacteria in sheets and in dissociated single flagellates (**Figure 4O** and **S16B**). We found that sheets captured more than twice as many fluorescent bacteria per cell as single cells (**Figure 4O**). This suggests that multicellularity confers a prey capture advantage at salinities compatible with the maintenance of a functional collar complex, and therefore with feeding.

Clonal-aggregative multicellularity is a versatile strategy for robust re-establishment of multicellularity in a variable environment

Although splash pools all undergo similar evaporation-refilling cycles, they vary in size, evaporation rate, and salinity after refilling. Given this variability, we wondered whether

333 environmental parameters might shift the relative contributions of clonality and aggregation.
334 Notably, we reasoned that conditions that impair cell division might favour aggregation,
335 whereas conditions that limit cell-cell encounters might favour clonal multicellularity.

336 We first examined the influence of salinity within the range compatible with
337 multicellularity (*i.e.,* below the dissociation-encystation threshold). At seawater salinity (1X),
338 both cell division and aggregation occurred (**Figure 5A** and **S17A**). By contrast, medium-high
339 salinity (2X) arrested cell division but did not affect aggregation (**Figure 5A** and **S17A**). Thus,
340 *C. flexa* sheets formed through mixed clonal-aggregative multicellularity at 1X salinity, but
341 through pure aggregation at 2X salinity.

342 We next examined the effect of cell density, reasoning that it might influence
343 aggregation efficiency by modulating encounter rates between cells. Field measurements
344 across 12 splash pools revealed densities ranging from 30 to $4.4*10^4$ cells/mL (**Figure S17B;**
345 **Table S1;** see Materials and Methods). This range overlapped with cell concentrations used
346 in laboratory aggregation experiments (from $1.0*10^4$ to $6.7*10^5$ cells/mL), confirming that *C.*
347 *flexa* can reach densities sufficient for aggregation in nature. To quantify the effect of cell
348 density, we seeded dissociated cells at 10^2 to 10^5 cells/mL under both 1X and 2X salinity. We
349 assessed aggregation efficiency by measuring final colony size under purely aggregative
350 conditions (2X salinity), and clonality efficiency by quantifying additional colony growth at 1X
351 salinity over the 2X baseline (see Materials and Methods). Measurements were taken during
352 early sheet formation to avoid saturation effects. Aggregation efficiency increased
353 monotonically with cell density and peaked at the highest density tested (10^5 cells/mL) (**Figure**
354 **5B** and **S17C**). By contrast, clonality efficiency remained constant across intermediate
355 densities (10^2-10^4 cells/mL) but decreased at the highest density (10^5 cells/mL), likely due to
356 depletion of bacterial prey limiting proliferation (**Figure 5B** and **S17C**). Therefore, low
357 densities favour clonal multicellularity, high densities favour aggregative multicellularity, and
358 intermediate densities support mixed clonal-aggregative formation.

359 Taken together, these data show that clonal-aggregative multicellularity spans a
360 spectrum along which environmental conditions modulate the relative contributions of clonality
361 and aggregation (**Figure 5C**). Importantly, certain environmentally relevant conditions – such
362 as medium-high salinity or extreme cell densities – suppress one mode, resulting in purely
363 clonal or purely aggregative multicellularity. This plasticity thus allows *C. flexa* to achieve
364 multicellularity across a broader environmental range than either mechanism alone would
365 permit.
366

367 ***C. flexa* sheets formed by aggregation are equivalent to control sheets in**
368 **morphology and behaviour**
369
370 Having identified environmentally relevant conditions that modulate the balance between
371 clonal and aggregative multicellularity, we next asked whether *C. flexa* colonies formed by
372 aggregation are functionally equivalent to those formed by cell division. We set out to
373 characterise purely aggregative sheets, obtained by seeding dissociated cells at high density
374 under 2X salinity. These were compared to control sheets generated under conditions
375 permissive for clonality (1X salinity and a low initial density of 200 cells/mL; see Materials and
376 Methods). Both control and aggregative sheets exhibited a similar polarised monolayer
377 structure (**Figures 5D-E** and **S17D-G**) and were statistically indistinguishable in size (**Figure**
378 **S17H**), proportion of aligned cells (**Figure S17I**), collar-collar angles (**Figure 5F** and **S17I'**),
379 and circularity (**Figures 5F'** and **S17J**).
380 To test whether aggregation could also support the growth of pre-formed colonies
381 independently of cell division, we fluorescently labelled single cells and added them to pre-
382 formed sheets under 2X salinity (**Figure S18A**). The labelled cells initially adhered at the
383 periphery of the sheets in variable orientations (**Figure S18B-C,F**) but, after 24 hours, they
384 were robustly incorporated into the pre-existing colonies, displaying collar-collar contacts and
385 aligned apico-basal polarity with their unlabelled neighbours (**Figure S18D-F**). These
386 observations show that aggregation alone is sufficient to support both the formation and
387 growth of sheets with wild-type morphology, independently of cell division.
388 We then characterised the behaviour of purely aggregative sheets. Both control and
389 aggregative sheets exhibited equivalent inversion behaviour in response to light-to-dark
390 transitions (**Figures 5G** and **S19**) and comparable prey capture efficiency over single cells
391 (**Figure 5H**). In an independent assay, we also generated sheets by aggregation of cells
392 labelled with two different colours (as in **Figure 2H**) and confirmed that the resulting chimeric
393 sheets robustly inverted in response to light-to-dark transitions (**Movie S19**). These results
394 demonstrate that *C. flexa* can form fully functional colonies through aggregation alone.
395 Thus, although environmental parameters modulate the strategy by which *C. flexa*
396 becomes multicellular, the morphology and behaviour of the resulting sheets appear largely
397 uncoupled from their formation mechanism.
398
399 **Aggregation is species-specific and constrained by kin recognition**
400

401 To assess the relevance of aggregation in the life history of *C. flexa*, we tested for
402 biological signatures of aggregative multicellularity. A frequent feature of this process is
403 species specificity, whereby cells aggregate preferentially with their own species and little or
404 not at all with others[65]. We tested this by mixing equal quantities of *C. flexa* and *S. rosetta*
405 single cells. *C. flexa* formed aggregative sheets that completely excluded *S. rosetta*,
406 demonstrating species-specific aggregation (**Figure S20**). Notably, *S. rosetta* cells did not
407 aggregate with each other under these conditions, confirming that aggregation is specific to
408 *C. flexa* rather than a general behaviour of choanoflagellate cells at sufficient density.
409 A second frequent feature of aggregative multicellularity is kin recognition – *i.e.,* the ability
410 to discriminate kin versus non-kin and to preferentially aggregate with closely related strains
411 within the same species. Kin recognition increases genetic homogeneity within the resulting
412 multicellular entity, which is thought to facilitate the evolution of coordinated collective
413 behaviour[66] and/or restrict the spread of cheater mutants[16]. We assessed kin recognition
414 among three *C. flexa* strains isolated from different splash pools: Strain 1 (originally isolated
415 in 2019 and used in laboratory experiments above), and Strains 2 and 3 (both isolated in 2023
416 during Exped-B; **Figure 6A-B**). Each strain was established by manual isolation of a single
417 sheet, followed by amplification in laboratory cultures (referred to as 'single-sheet-
418 bottlenecked' cultures). Isolation of single cells from each single-sheet-bottlenecked culture
419 allowed the establishment of clonal strains (referred to as 'single-cell-bottlenecked cultures'
420 or 'clones').
421 To test for genetic divergence between these strains, we first sequenced, assembled, and
422 annotated the *C. flexa* reference genome using a combination of long-read and Omni-C
423 sequencing. The final assembly comprised 56 Mb and 14,084 genes across 528 scaffolds,
424 with a BUSCO completeness score of 82.8%. This represents the third high-quality
425 choanoflagellate genome after *M. brevicollis*[74] and *S. rosetta*[67,68]. We then performed short-
426 read sequencing of Strains 1, 2 and 3, as well as of three clonal descendants of each strain.
427 Across all samples, we detected 193,564 SNPs, allowing us to reconstruct a phylogenomic
428 tree in which all three parent strains were clearly delineated from each other (**Figure 6C** and
429 **Supplementary Files S5,S6**). All clones clustered with their strain of origin with strong
430 support and contained similar levels of genetic diversity to their corresponding single-sheet-
431 bottlenecked strain (**Figure S21**). These results suggest either clonal formation of the
432 originally isolated sheets (as in **Figure 1E-G**) or a loss of genetic diversity during sheet
433 isolation and establishment of laboratory cultures (see Materials and Methods).

434 We tested kin recognition by dissociating sheets from all three strains, staining them with
435 different fluorophores, and assessing aggregation across all pairwise strain combinations
436 seeded at equal initial cell density (as in **Figure 2H**). All strains aggregated within hours,
437 confirming that aggregation is a widespread behaviour among independently isolated *C. flexa*
438 strains. Interestingly, cells of Strains 1 and 2 preferentially aggregated with their own strain
439 when mixed, indicating kin recognition (**Figures 6D-G** and **S22**). By contrast, other pairwise
440 combinations of strains showed no quantifiable preference for self-aggregation and readily
441 formed chimeric sheets, as did cells of the same strain stained with different fluorophores
442 (consistent with earlier results; **Figures 2H** and **S3**).
443 These results suggest the existence of a kin recognition system in *C. flexa*, reminiscent of
444 those described in other aggregative multicellular organisms such as dictyostelid social
445 amoebae. In the latter, kin recognition is mediated by polymorphic surface receptors rich in
446 immunoglobulin and other adhesion domains[18,69]. In *Dictyostelium*, such receptors were first
447 identified by their high ratio of non-synonymous to synonymous substitutions (Ka/Ks), a
448 signature of diversifying selection[18]. We reasoned that, if *C. flexa* indeed possesses a
449 comparable kin recognition mechanism, candidate kin recognition loci might be revealed by
450 screening the genomes of Strains 1 and 2 for high Ka/Ks loci. Across all pairwise strain
451 comparisons, we identified 840 genes with high Ka/Ks regions (**Figure 6H**), including multiple
452 transmembrane proteins (**Figure S23A**). These high Ka/Ks genes encoded predicted proteins
453 with a significant overrepresentation of domains consistent with adhesion (cadherins, TM132)
454 or signalling (protein kinase) functions (**Figures 6I** and **S23B**). The most promising kin
455 recognition candidates notably included one predicted cadherin (FUN_000880; **Figure 6I-J)**
456 and one predicted receptor-protein kinase (FUN_003087; **Figures 6I** and **S23B-C**) that
457 displayed particularly strong signatures of diversifying selection between Strains 1 and 2.
458 These findings indicate that polymorphic receptor candidates potentially mediating kin
459 recognition can be readily identified in *C. flexa*, although some of these proteins may perform
460 other functions, such as capture of bacterial prey. Determining their precise roles will require
461 functional genetic tools, which are not yet available for *C. flexa*.
462 Taken together, species-specificity and kin recognition support the view that aggregation
463 is a regulated biological process in *C. flexa*.
464
465 **Discussion**
466

467 Our findings suggest that evaporation-refilling cycles of splash pools, the natural habitat
468 of *C. flexa*, regulate its clonal-aggregative multicellularity (**Figure 6K**). *C. flexa* sheets are
469 found in water-filled splash pools with salinities up to ~3-fold that of natural seawater. As
470 gradual evaporation proceeds, salinity increases, and sheets dissociate, with cells
471 differentiating into solitary, non-motile, non-proliferative cysts. These cysts can survive
472 complete desiccation and persist in the soil of the splash pools. Upon splash pool refilling,
473 cysts regenerate a collar complex and transition back into free-swimming flagellates, which
474 re-form multicellular sheets through aggregation and/or clonal division. This mixed
475 mechanism confers two key advantages in this environment: (i) robust re-establishment of
476 multicellularity across a broad range of conditions, and (ii) fast acquisition of multicellularity
477 by simultaneous action of both mechanisms. Indeed, aggregation generally provides a speed
478 advantage over clonality, as aggregative eukaryotes often complete multicellular formation
479 within a few hours[20,20,70], whereas clonal multicellularity is constrained by cell cycle duration,
480 which ranges from one to eleven days in diverse micro-organisms in the wild (**Table S3**).
481 Thus, the ability of *C. flexa* to aggregate may therefore allow faster and more robust re-
482 establishment of multicellularity in the variable and ephemeral environment of splash pools.
483 The environmentally entrained life history of *C. flexa* parallels other recently described
484 examples in which unicellular-to-multicellular transitions are modulated by fluctuating
485 environmental parameters, such as salinity in cyanobacteria inhabiting brackish
486 environments[71] and periodic flooding in cave-dwelling bacteria[72]. A selective advantage for
487 regulated life cycles in fluctuating environments is also supported by laboratory experiments
488 in yeast[73] and by theoretical models[5,74,75]. The environmentally entrained life cycle of *C. flexa*
489 may thus allow it to combine both the benefits of multicellularity (enhanced filter-feeding,
490 presumably supporting faster proliferation) with those of the unicellular cyst form (resistance
491 to desiccation).
492 The ability of *C. flexa* to aggregate contrasts with prevailing views of choanoflagellates,
493 which are canonically considered to exhibit strictly clonal multicellularity[25,39,76–78] – like animals,
494 their sister-group. Our study therefore reveals unexpected diversity in the modes of
495 multicellularity within a pivotal clade for reconstituting animal origins. Notably, strictly clonal
496 multicellularity has so far been experimentally demonstrated in only a single choanoflagellate
497 species, the model *S. rosetta*[39]. This suggests that the diversity of choanoflagellate
498 multicellularity warrants more systematic re-exploration. Although incomplete character-state
499 mapping currently limits ancestral-state reconstruction, broader taxonomic sampling in the
500 future will ultimately clarify whether clonal-aggregative multicellularity contributed to the

501 origins of animals (as proposed by some authors[27]) or represents a specific innovation of the
502 *C. flexa* lineage.

503 The mixed clonal-aggregative multicellularity of *C. flexa* was a surprise, given that
504 clonal and aggregative multicellularity are often depicted as mutually exclusive in
505 holozoans[2,79] and eukaryotes in general[80–82]. However, although clonal-aggregative
506 multicellularity has not previously been reported in close relatives of animals, nor in the context
507 of a regulated life cycle to our knowledge, clonality and aggregation occasionally cooperate
508 in the formation of other biological structures. These include bacterial biofilms[83],
509 experimentally evolved clusters of bacteria[84], predator-induced groups of freshwater algae
510 (which can even combine different species)[10], clusters of budding yeast[85], and certain
511 syncytial amoebae[19]. While these diverse processes may not all represent *bona fide*
512 multicellularity[86] – since the resulting structures often lack multicellular-level adaptations such
513 as controlled shape, size, or collective behaviour – they demonstrate that aggregation and
514 incomplete cell division can coexist. Clonal-aggregative multicellularity may therefore be more
515 widespread than currently appreciated.

516 Aggregation presents a well-known evolutionary challenge: a single aggregate can
517 combine cells of different ancestries and potentially different genotypes, creating the potential
518 for genetic conflict[87–89] and, perhaps more importantly, limiting the coevolution of genes
519 required for the emergence of complex multicellular behaviours[66,90]. The risks of chimerism
520 can be mitigated if aggregation is restricted to close relatives – either actively, through kin
521 recognition mechanisms, or passively, through a spatially structured environment limiting
522 dispersal[91,92]. The latter might be relevant to *C. flexa*, as splash pools are collections of
523 physically disconnected environments that might promote geographic divergence of
524 genotypes, as shown for other organisms in similar environments (*e.g., Daphnia*
525 metapopulations in tide pools[93]). Splash pools may thus have favoured the evolution of
526 aggregative multicellularity by initially relaxing selection for strong kin recognition mechanisms
527 (which *C. flexa* nonetheless appears to have eventually evolved). This scenario aligns with
528 the emerging concept of 'ecological scaffolding', which proposes that patchy environments
529 can facilitate the emergence of multicellularity by fostering local cooperation[94]. In the future,
530 these questions will be informed by deeper characterization of dispersal, molecular kin
531 recognition mechanisms, and natural genetic diversity at different scales (within and between
532 colonies, within and between splash pools) in *C. flexa*.

533 The complex life history of *C. flexa* illustrates the phenotypic plasticity of close
534 unicellular relatives of animals and thus lends additional support to the emerging concept of

a pre-metazoan origin for complex life cycles[21,95]. Beyond this, our study establishes *C. flexa* as a powerful model to study the establishment of multicellularity in a close relative of animals within its natural context. This contrasts with other well-characterised facultatively multicellular holozoans, such as *S. rosetta*[22] and *C. owczarzaki*[96], which were each isolated only once from their natural environment over two decades ago, inevitably restricting studies of unicellular-to-multicellular transitions in these species to laboratory settings. In the future, we expect the continued dialogue between field and laboratory studies of *C. flexa* to continue clarifying key questions, such as the selective advantage(s) and ecological consequences of multicellularity versus unicellularity, the evolvability of clonal-aggregative behaviours under diverse selective pressures in diverse environments, and the molecular mechanisms of kin recognition.

Data availability

The annotated reference *C. flexa* genome has been deposited on Zenodo under doi: 10.5281/zenodo.13837466. Raw short reads for Strains 1, 2 and 3 have been deposited on Zenodo under doi: 10.5281/zenodo.13837614.

Code availability

The codes used for SNP analysis are deposited on Github:
https://github.com/uhoro/RRRR_SNP_analysis

Acknowledgements

We enormously thank Nicole King for support during this project and for providing useful feedback. We thank the personnel of the Shete Boka National Park in Curaçao for access to the field site. Special thanks to Tess Linden for help during preliminary field experiments and feedback on the manuscript, as well as to Geneviève Milon and Noah Whiteman for advice on laboratory and field experiments, respectively. Thanks to David S. Booth for providing JRR with access to microscopes and lab space during revision of this work after peer-review. Yashraj Chavhan, Seemay Chou, Stefania Kapsetaki, and Iñaki Ruiz-Trillo and members from the Multicellgenome lab that provided useful feedback on the preprint version of the manuscript. Marvin Albert, Stéphane Rigaud and Jean-Yves Tinevez at the Image Analysis Hub at the Institut Pasteur provided advice on image analysis. Pierre-Henri Commere and Sebastien Megharba from the Flow Cytometry platform at Institut Pasteur provided technical support with single-cell isolation of *C. flexa* by flow cytometry. We acknowledge the help of the HPC Core Facility of the Institut Pasteur for bioinformatic analyses. We thank Thomas Swale (Dovetail Genomics/Cantata) and Tara Rickman (Phase Genomics) for help with genome sequencing and assembly and for drafting the relevant Methods sections. We also thank members of Brunet and King laboratories for feedback and useful discussions and Jaime Ramirez and Kayla Dinshaw for technical support during preliminary experiments. NRR is supported by the European Union's Horizon Europe research and innovation funding program under a Marie Skłodowska-Curie Actions grant (FlexAggon, grant agreement ID: 101106415). JRR is supported by a National Science Foundation Graduate

Research Fellowship Program (grant no. 1752814) and the National Science Foundation Postdoctoral Research Fellowship in Biology (grant no. 2507925). UH is supported by the PPU program of the Institut Pasteur. Work in the King lab (TB, JRR, BTL, MCC) is supported by the Howard Hughes Medical Institute. JLS is a Howard Hughes Medical Institute Awardee of the Life Sciences Research Foundation. TB and work in the Brunet lab are supported by the Institut Pasteur (G5 package), the ERC (EvoMorphoCell, grant agreement ID: 101040745), the Vallee Foundation Inc, and the CNRS (UMR 3691). Views and opinions expressed are, however, those of the author(s) only and do not necessarily reflect those of the European Union or the European Research Council. Neither the European Union nor the granting authority can be held responsible for them.

Author contributions

NRR, JRR, TB conceptualised the study and coordinated the work. MCC, BTL and TB performed preliminary fieldwork that identified the Shete Boka site that gave first insights in the *C. flexa* salinity range. NRR, JRR and TB collected fieldwork data included in this study. NRR, JRR and TB performed all laboratory experiments, strain isolations and bioinformatic analyses (except those specified below). BTL performed preliminary aggregation assays and aphidicolin treatments. YF optimised live imaging of dual-labelling aggregation experiments and performed growth curves under addition of salts under the supervision of NRR. JLS performed genome assembly and annotation. UH performed behavioural assays with technical support from NRR and SNP analyses with technical guidance from JLS. CC performed single-cell bottleneck isolations and generated the material for genome sequencing of Strains 1, 2 and 3. EATH and MAV provided support for fieldwork studies. EATH performed drone orthomap imagery. JRR wrote the first draft of the manuscript which was subsequently edited by NRR and TB. NRR made the figures with feedback from JRR and TB. TB supervised the study. All authors contributed to the review of the manuscript before submission for publication and approved the final version.

Inclusion & ethics statement

All Curaçao researchers who supported or performed fieldwork are authors of the present manuscript.

Competing interests

JLS is an advisor for ForensisGroup Inc.

Materials and Methods

See detailed Materials and Methods in the **Supplementary Information** file.

Supplementary Material

Supplementary **Figures S1-S23**, **Tables S2-S3** and legends for **Table S1**, **Supplementary Files S1-S6** and **Supplementary Movies S1-S19** are provided in the **Supplementary Information** file.

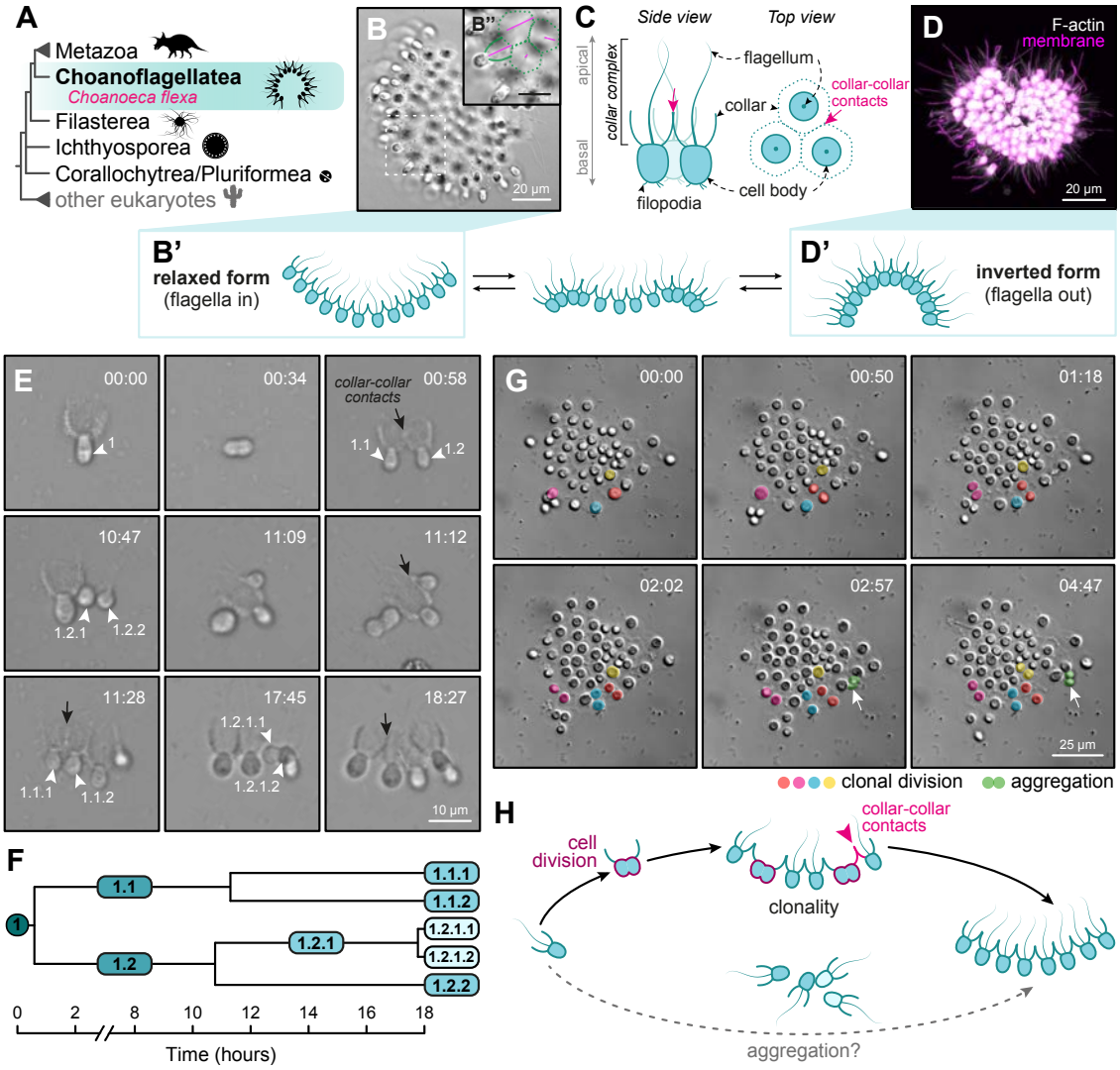

Figure 1. *Choanoeca flexa* sheets can form clonally but display aggregative features. (A) Choanoflagellates (turquoise) are the sister group to animals (Metazoa). The phylogenetic relationships depicted are based on several recent phylogenomic studies[14,97]. Uncertain positions are represented with polytomies. (B) Brightfield image of a *C. flexa* multicellular colony ("sheet") in its relaxed conformation (B'). B", dashed square: zoom-in showing flagella (magenta pseudocolour) and direct collar-collar contacts between cells (green pseudocolour). Scale bar in B'': 10 µm. (C) Diagnostic morphological features of a choanoflagellate cell. *C. flexa* cells within a sheet are linked by their collars (magenta arrow). (D) 3D reconstruction of an Airyscan confocal Z-stack of a fixed sheet exhibiting an inverted conformation (D'), with cell bodies stained with a membrane/cytoplasmic dye (FM 1-43FX, magenta, which distributes to the membrane and cytoplasm of cells following fixation), and collars stained with a filamentous actin (F-actin) dye (Phalloidin-Rhodamine, white). (E) Stills from a brightfield timelapse movie of clonal *C. flexa* sheet formation by serial cell division from a single *C. flexa* swimmer cell (white arrowhead). After each division, the sister cells remain adhered to each other by direct collar-collar contacts between cells (black arrow). Note that cells retract their flagellum during division. Time scale hh:mm. (F) Cell lineage tracing as a function of time in E shows that cells divide asynchronously during colony formation, taking ~8-10 hours between each round of division. (G) Stills from a brightfield

timelapse movie depicting a medium-sized *C. flexa* sheet (flagella-in conformation) that expands in cell number both by cell division (pseudocolours in orange, pink, blue and yellow) and by cellular aggregation (white arrow, pseudocolour in green). Time is hh:mm. (H) Schematics of *C. flexa* clonal multicellularity observed under laboratory culture conditions: unicellular flagellate (swimmer) cells can divide clonally to initiate a colony; in turn, colonies can increase in cell number by clonal division. Sister cells resulting from cell division adhere to each other through direct collar-collar contacts between cells (magenta arrowhead). The hypothesis that *C. flexa* sheets might be able to form purely by aggregation is tested in **Figure 2**. Figure related to **Figure S1** and **movies S1-S3**.

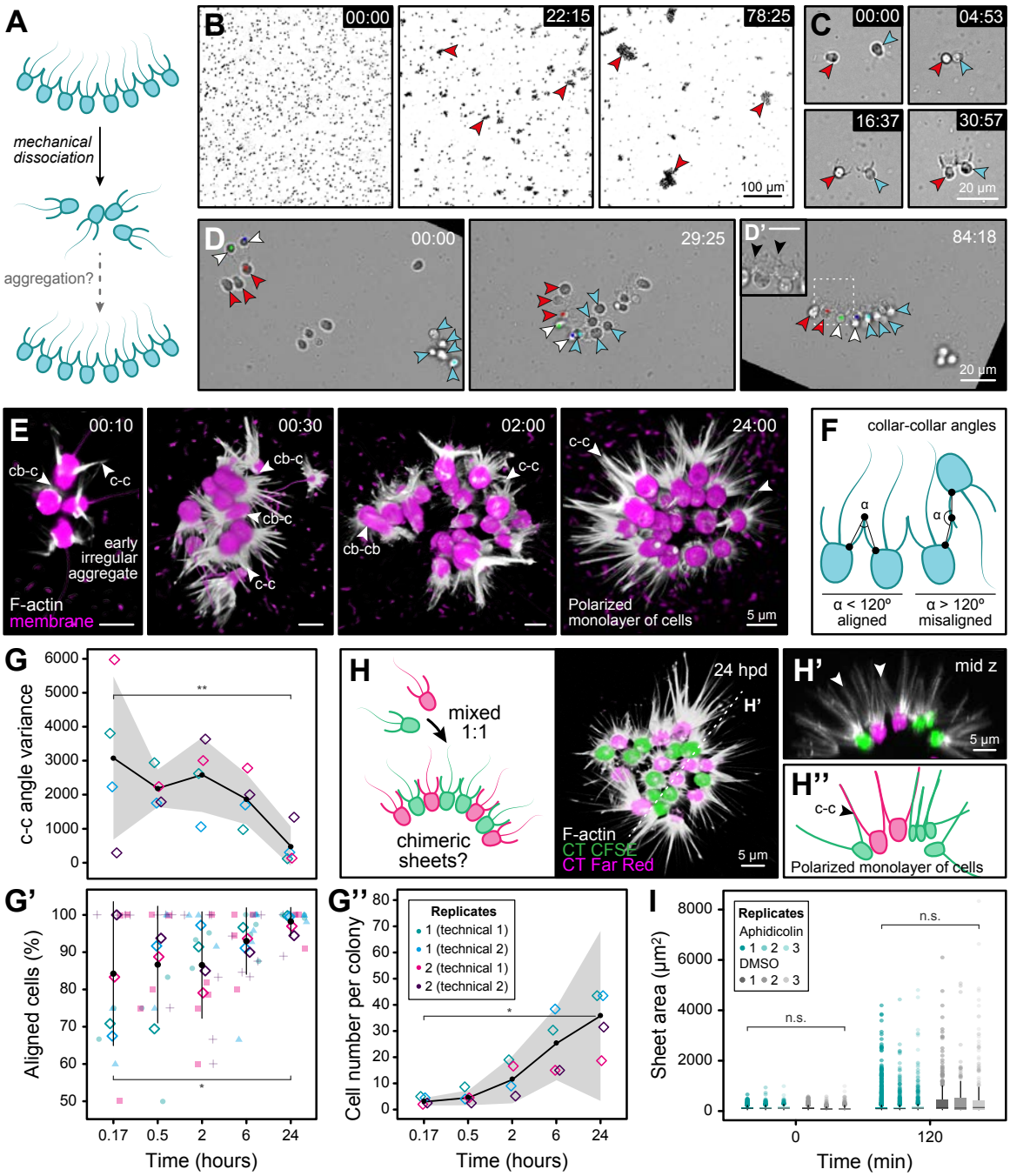

Figure 2. *C. flexa* sheets can form by aggregation.

(A) Experimental pipeline. Mechanical dissociation of colonies into single cells is followed by live imaging. (B) Dissociated flagellate cells form aggregates (red arrowheads) within minutes. Stills from Movie S4. Upper right: time. (C) Two dissociated flagellate cells (red and blue arrowheads) aggregating into a doublet connected by collar-collar contact. Stills from Movie S5. Upper right: time. (D) A cell doublet (white arrowheads) and two small sheets (red and blue arrowheads) at t=0 (left, pre-aggregation) aggregate into a larger sheet. The aggregate initially comprises cells with diverse orientations (middle, irregular aggregate) but later matures into a polarised monolayer showing cells with the same apico-basal orientation connected by collar-collar contacts (right, mature aggregate).

649 Stills from Movie S6. Upper right: time. (D') Dashed square: closeup of the area in the white dotted
650 square in D, showing collar-collar contacts (black arrowheads). Scale bar: 10 µm. Timescales in B-D:
651 mm:ss. (E) 3D reconstruction of Airyscan confocal z-stacks of dissociated flagellate cells fixed after 10
652 minutes (n=11), 30 minutes (n=14), 2 hours (n=17), and 24 hours (n=13) of aggregation, stained for
653 membrane/cytoplasm (FM 4-64FX, magenta) and F-actin (phalloidin, white). Note that cells frequently
654 show unaligned apico-basal polarity and diverse cell orientations at early timepoints, but almost
655 exclusively collar-collar contacts at late timepoints (white arrowheads; cb-c: cell body-collar contacts,
656 cb-cb: cell body-cell body contacts, c-c: collar-collar contacts). Time scale: hh:mm. (F) Schematics of
657 the morphological metrics quantified from the cells in E: adhesion angle between collar-collar contacts
658 of neighbouring cells (α) and proportion of cells with aligned apico-basal polarity. (G) Quantification of
659 collar-collar angle variance between cells during aggregation in E. (G') Quantification of percentage of
660 aligned cells within colonies in E. (G'') Quantification of cell number per colony during aggregation in
661 E. Black circles: mean; error bars and grey ribbon: standard deviation; diamonds: mean values of each
662 independent replicate. (H) (Left panel) Dissociated single flagellate cells labelled with CellTrace CFSE
663 (green) or CellTrace Far Red (magenta) and mixed at a 1:1 ratio will form chimeric sheets 24 hours
664 post-dissociation (hpd) if aggregation occurs. (Right panel) 3D reconstruction of Airyscan confocal z-
665 stacks of a sheet formed by aggregation from dissociated flagellated cells labelled as depicted before
666 and fixed 24 hpd, with additional F-actin staining (phalloidin, white). (H') Mid z cross-section (dashed
667 line) in H. Note that cells within the chimeric sheet are connected by collar-collar contacts (white
668 arrowheads) and maintain their apico-basal polarity. (H'') Schematics of H', showing a polarised
669 monolayer of cells and collar-collar contacts (c-c) of the chimeric sheet in H. (I) Quantification of particle
670 area during an aggregation time course of dissociated single cells pre-treated with 17 µg/mL Aphidicolin
671 overnight or the equivalent volume of a DMSO (dimethyl sulfoxide) control (n=9). Statistics in G-G''
672 (comparing t=10 min and t=24 h) and I (comparing average area of Aphidicolin-treated versus DMSO
673 control at each timepoint) by the Mann-Whitney U test (* for $p<0.05$; ** for $p<0.01$; *** for $p<0.001$; n.s.,
674 non-significant). Statistics in G' by linear regression: adjusted $R^2 = 0.081$, p-value= 0.042. Figure related
675 to **Figures S2-S5** and **movies S4-S13**.
676

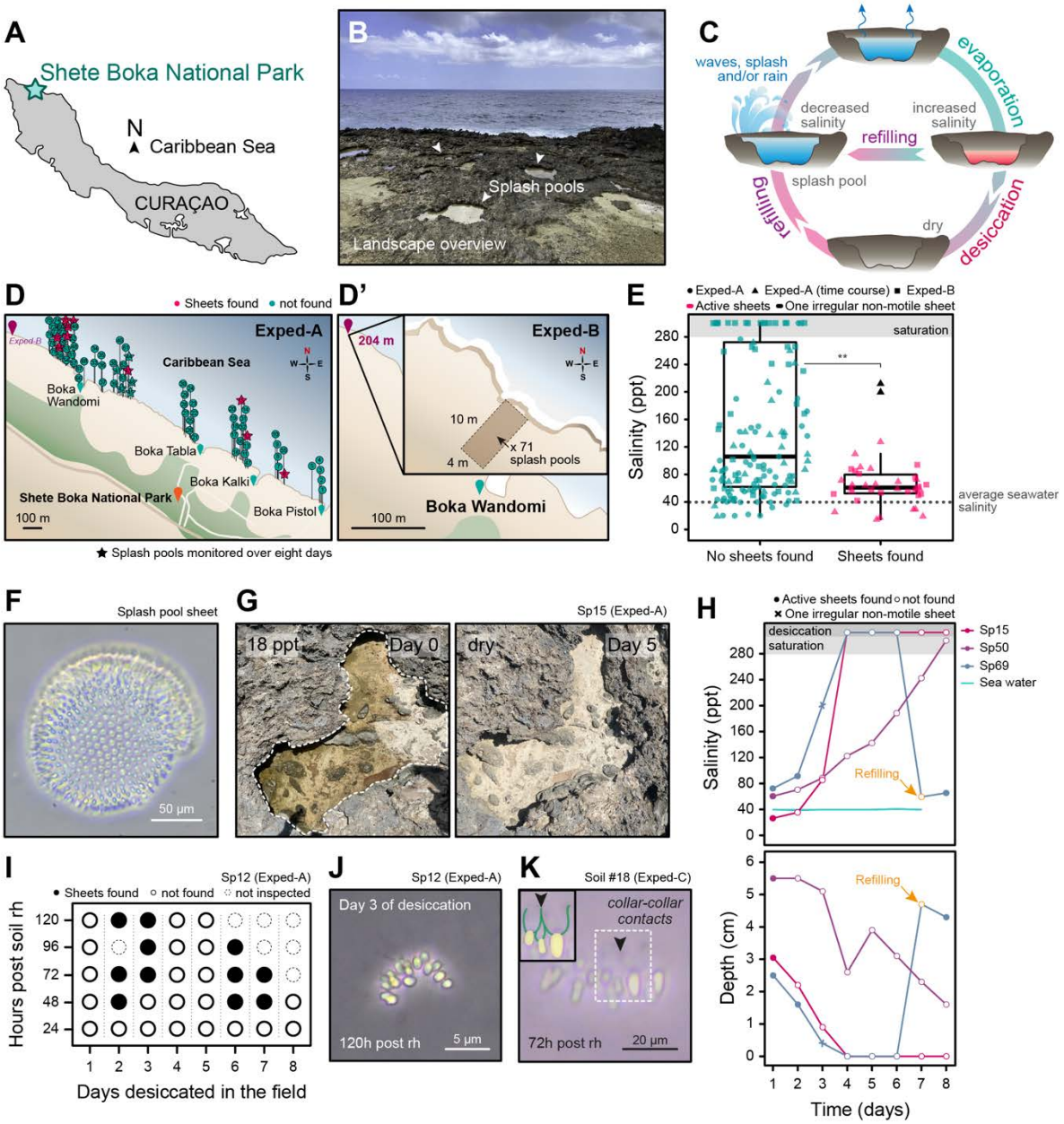

Figure 3. Natural evaporation-refilling cycles constrain the occurrence of multicellular *C. flexa* in the wild.

(A) Map of Curaçao and location of Shete Boka National Park (turquoise star) where fieldwork data were collected in Exped-A and Exped-B (12° 22' 5.718" N, 69° 06' 56.916" W). (B) Representative photograph of the landscape in Shete Boka, including splash pools where *C. flexa* sheets can be found (white arrowheads). (C) Schematic of the natural cycle of splash pool evaporation, desiccation, and refilling. (D) Maps showing the locations of sampled splash pools in Exped-A and in Exped-B. In Exped-A (D), samples were collected from splash pools along ~2 km of Shete Boka coastline (n=79). 10 splash pools with sheets and 5 without sheets on Day 1 were randomly selected for daily monitoring during eight days (stars). Colours indicate whether sheets were found (magenta) or not found (turquoise) on Day 1. In Exped-B (D'), a random number generator was used to select the randomised sampling

location (purple pin, 204 m upstream of Boka Wandomi). Samples were collected from splash pools within a 10 m x 4 m area (n=71). (E) Distribution of salinity of splash pools surveyed in Exped-A (circles), Exped-A time course (triangles), and Exped-B (squares). For Exped-A time course, all measurements are shown, except for those where splash pools were dry. The observed natural limit of salinity where active sheets were found (128 ppt) and the average seawater salinity measured in the *bokas* are indicated with grey dotted lines. Grey area: salinity saturation (>280 ppt). (F) Brightfield image of a sheet observed in a splash pool sample (n=18). (G) Representative images of a splash pool near Boka Kalki (Sp15) followed for eight days, showing recorded salinity in the upper left. This splash pool was partially evaporated on day 0 (left) and completely desiccated on day 5 (right). Dashed line: splash pool outline. (H) Salinity (upper panel) and depth (lower panel) measurements in three representative splash pools followed over eight days (n=15). Shown are one splash pool that experienced evaporation but not complete desiccation (Sp50), one splash pool that experienced complete desiccation (Sp15), and one splash pool that experienced both desiccation and refilling (Sp69). (I) Recovery of sheets from soil samples collected from a splash pool (Sp12 from Exped-A) when desiccated. Soil samples were collected every day for eight days and were independently rehydrated in the laboratory with filtered natural seawater. Each rehydrated soil sample was monitored over five days for sheet re-appearance. rh: rehydration. Rehydration experiments were performed from soil collected in n=6 independent splash pools, with a minimum of three independent rehydrations each. (J) Brightfield image of a soil-recovered sheet (same experiment as in I) collected after 3 days of desiccation and rehydrated in the laboratory. (K) Brightfield image of a soil-recovered sheet independently collected and rehydrated from a splash pool sample (Soil #18) in Exped-C, showing collar-collar contacts (black arrowhead). Dashed square: detail of cell-cell contacts by the collars (black arrowhead). Green pseudocolour: collars; yellow pseudocolour: cell bodies. Rehydration experiment performed from soils collected in n=26 independent splash pools. Time post-rehydration in J-K is depicted in the lower left. Figure related to **Figures S6-S9**, **movies S14-S16**, **Tables S1-S2** and **Supplementary Files S1-S4**.

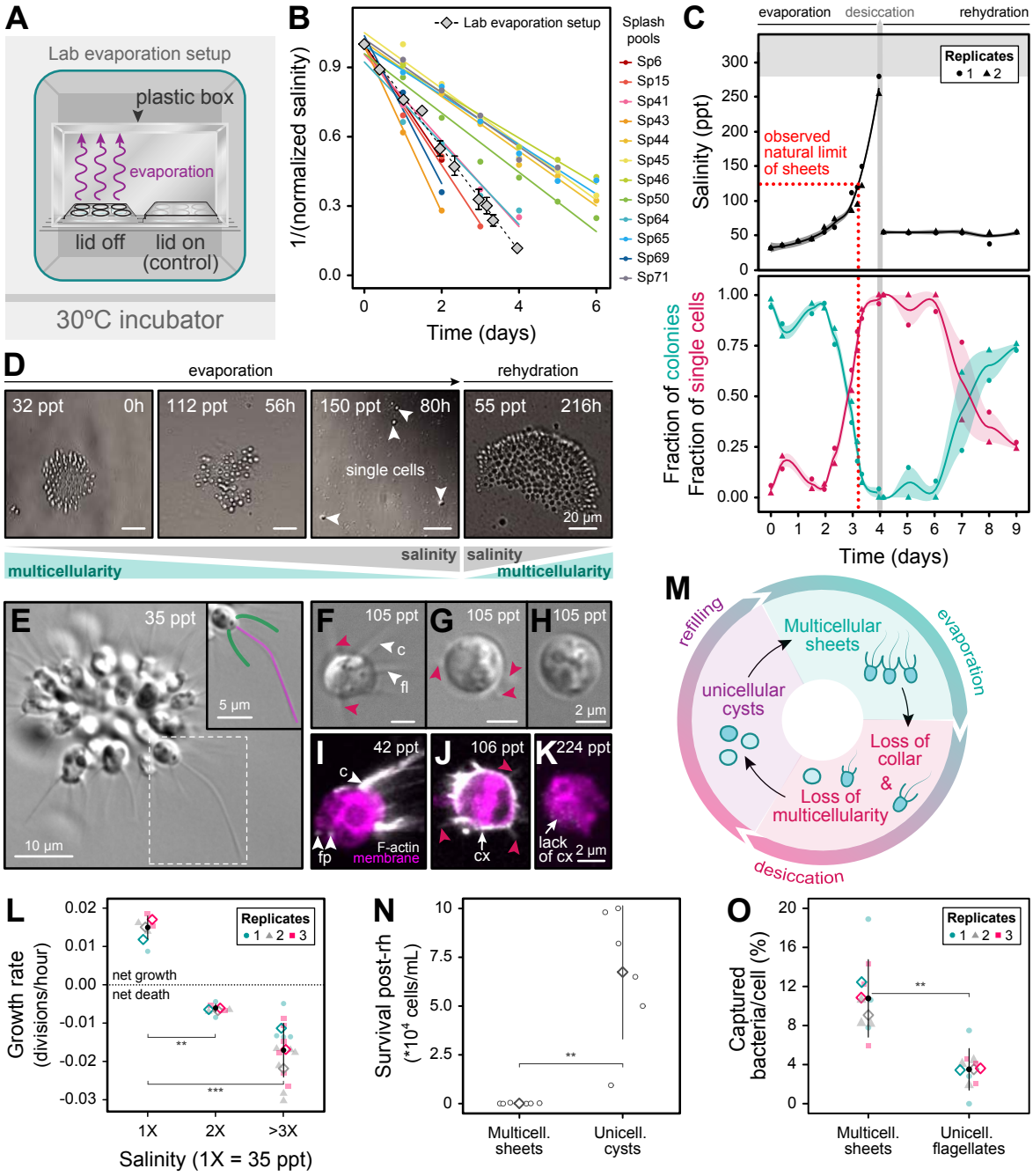

Figure 4. Experimental evaporation-refilling cycles cause reversible transitions in and out of multicellularity.

(A) Laboratory experimental evaporation setup in a 30ºC incubator. Lid-off plates (gradual evaporation condition) and lid-on plates (no-evaporation control) were placed on a grid to allow air renewal and covered with a plastic box to avoid contamination. (B) Salinity increases over time in 12 gradually evaporating splash pools (data from Exped-A time course; **Figures 3H** and **S8**) and in the laboratory evaporation setup in A. Splash pools with fewer than three points below saturation are not depicted (Sp12, Sp42, and Sp70; see **Figure S10**). (C) Quantification of salinity and fraction of cells in multicellular versus unicellular forms during a nine-day gradual evaporation time course. Lines: mean values. Ribbon: standard deviation. (D) Micrographs of *C. flexa* sheets during the gradual evaporation

experiment in C. Upper left: salinity. Upper right: time. Sheets had completely dissociated into single cells (white arrowheads) after 80 hours. Multicellular sheets were observed again after complete desiccation and rehydration with artificial seawater. (E-H) Brightfield images of *C. flexa* showing morphological changes during gradual evaporation. Upper right: salinity (in ppt). At 1X salinity (35 ppt, E), *C. flexa* occurs in multicellular sheets of flagellates (dashed square). Green pseudocolour: collar; magenta pseudocolour: flagellum. During gradual evaporation (F-H), sheets dissociate into unicellular cysts. Cysts often lack a collar (c) and a flagellum (fl) but can exhibit filopodia-like protrusions (magenta arrowheads). (I-K) Airyscan micrographs of *C. flexa* cells fixed during gradual evaporation stained with a membrane (FM 4-64FX, magenta) and F-actin (phalloidin) dyes, showing salinity (in ppt, upper right). A flagellate cell (I, low-evaporation control) exhibits distribution of F-actin in the collar (c, white arrowhead) and filopodia (fp, white arrowhead). Gradual evaporation triggers a morphological change from a flagellate to a cyst, showing filopodia-like protrusions (magenta arrowheads) and a transient actin cortex (cx) at early stages of evaporation (J, white arrow) which disappears as salinity approaches saturation (K). (L) Growth rate of cells at different salinities during gradual evaporation. Black circles: mean; error bars: standard deviation; diamonds: mean values of independent biological replicates. (M) Schematic summarizing loss of multicellularity and phenotypic changes experienced by *C. flexa* cells during gradual evaporation. (N) Quantification of cell survival after 12 hours of desiccation in multicellular sheets (n=6) to unicellular cysts (n=6). Diamonds: means; error bars: standard deviations. (O) *C. flexa* multicellular sheets are more efficient at capturing bacteria than unicellular flagellates. Number of labelled bacteria captured per flagellate cells in multicellular colonies (n=9) or in cultures of unicellular flagellates (n=9). Black circles: means; error bars: standard deviations; diamonds: means of independent biological replicates. Statistics in L, N, and O by the Mann-Whitney U test (* for $p<0.05$; ** for $p<0.01$; *** for $p<0.001$; n.s., non-significant). Figure related to **Figures S10-S16** and **movies S17-S18**.

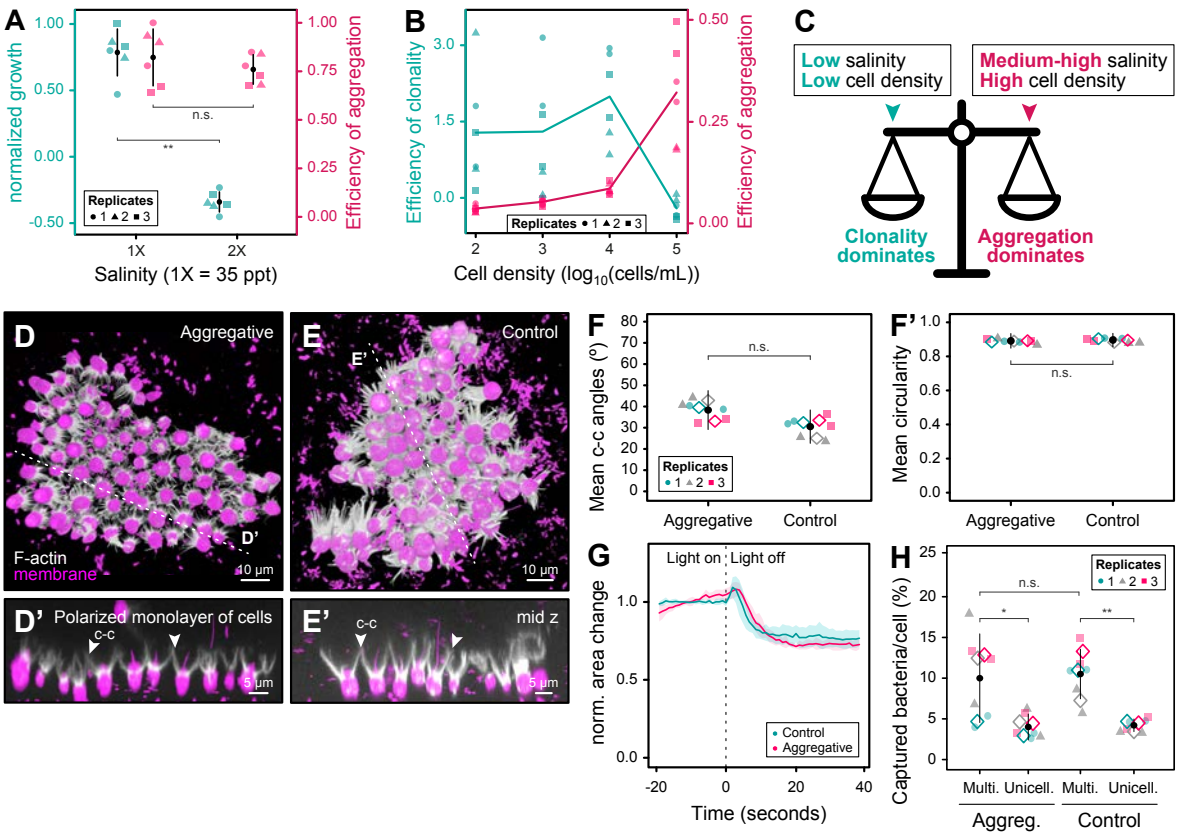

Figure 5. Environmental parameters modulate the relative contributions of clonality and aggregation.

(A) Normalised growth of *C. flexa* cells at different salinities during gradual evaporation (turquoise, left y-axis; from experiment in **Figure 4L**). Efficiency of aggregation of *C. flexa* cells at different salinities (magenta, right y-axis), calculated based on the area of sheets in a 2-hour time course experiment (see Materials and Methods). Black circles: mean; error bars: standard deviation. (B) Efficiency of clonality (turquoise, left y-axis) and aggregation (magenta, right y-axis) at different initial cell densities, based on the area of sheets in a 24-hour time course experiment (see Materials and Methods). Lines: mean. (C) Schematics illustrating the relative contributions of clonality and aggregation to *C. flexa* multicellularity, as modulated by environmental conditions. At low salinity and low cell density, clonality dominates, whereas at medium-high salinity and high density, aggregation dominates. (D-E) 3D reconstruction of Airyscan confocal z-stacks of purely aggregative sheets (D) and control sheets (E), stained for membrane/cytoplasm (FM 4-64FX, magenta) and F-actin (phalloidin, white). (D'-E') Mid z cross-sections (dashed lines) in D-E. Note that cells are connected by direct collar-collar contacts (c-c, white arrowheads), forming polarised monolayers of cells. (F) Quantification of mean collar-collar angles between cells in aggregative and control sheets in D-E. (F') Quantification of mean circularity of aggregative and control sheets in D-E. Black circles: mean; error bars: standard deviation; diamonds: mean values of each independent replicate (n=41 aggregative sheets; n=46 control sheets). (G) Normalised colony area changes before and after light-to-dark transitions (vertical dashed line, t=0) in control or purely aggregative sheets. Line: normalised mean area; ribbon: standard deviation. n=5 sheets quantified by condition. (H) *C. flexa* aggregative and control multicellular sheets are more efficient at capturing bacteria than unicellular flagellates. Experiment performed as in **Figure 4O**. Black circles: means; error bars: standard deviations; diamonds: means of independent biological replicates.

Statistics in A, F-F', and H by the Mann-Whitney U test (* for $p<0.05$; ** for $p<0.01$; *** for $p<0.001$; n.s., non-significant). Figure related to **Figures S17-S19** and **movie S19**.

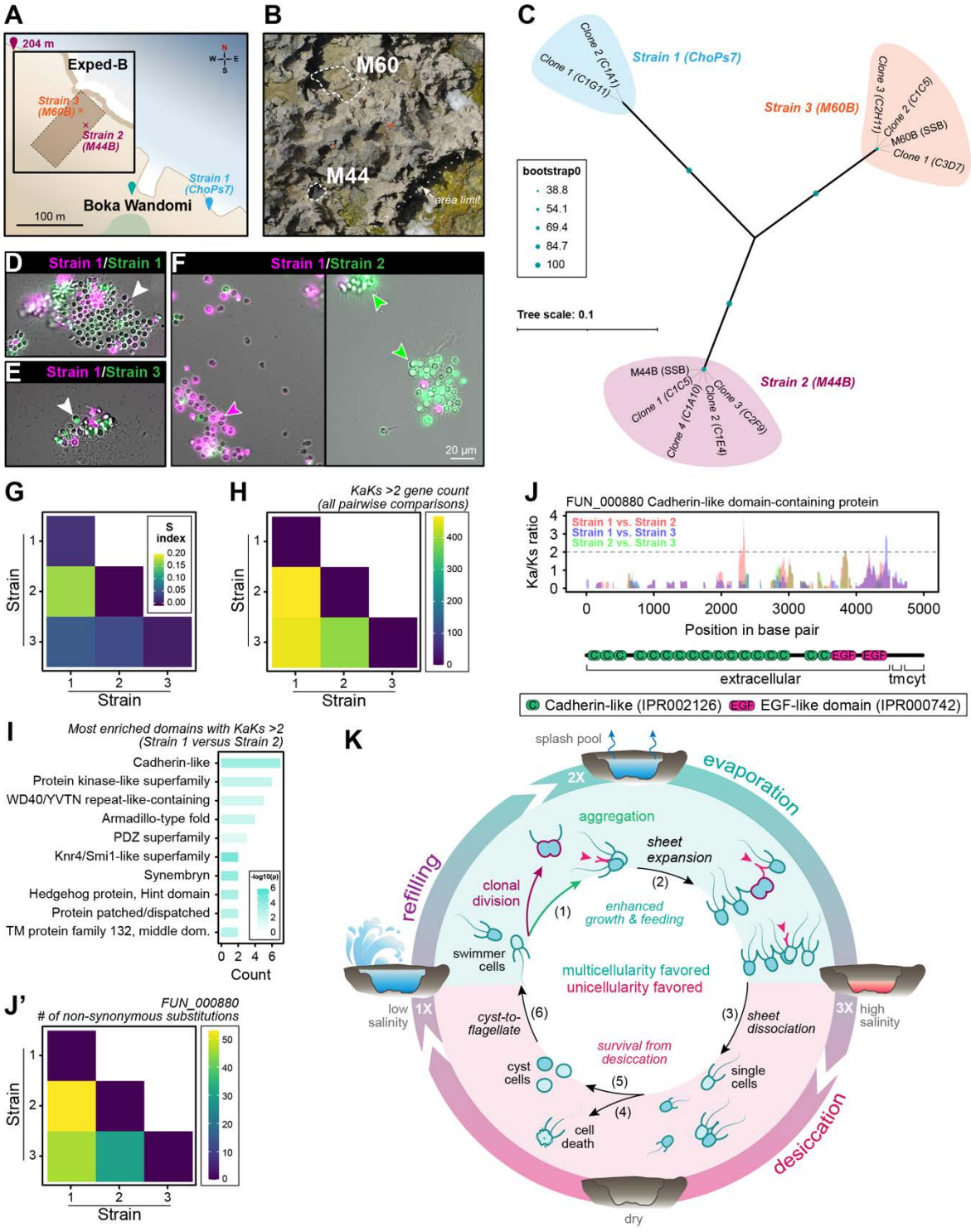
A
204 m
Exped-B
Strain 3 (M60B)
Strain 2 (M44B)
Strain 1 (ChoPs7)
Boka Wandomi
100 m
B
M60
M44
area limit
C
Strain 1 (ChoPs7)
Clone 2 (C1A1)
Clone 1 (C1G11)
Strain 3 (M60B)
Clone 3 (C2H11)
Clone 2 (C1C5)
M60B (SSB)
Clone 1 (C3D7)
bootstrap0
38.8
54.1
69.4
84.7
100
Tree scale: 0.1
Strain 2 (M44B)
M44B (SSB)
Clone 1 (C1C5)
Clone 4 (C1A10)
Clone 2 (C1E4)
Clone 3 (C2F9)
D Strain 1/Strain 1
E Strain 1/Strain 3
F Strain 1/Strain 2
20 µm
G
S index
Strain
H
KaKs >2 gene count (all pairwise comparisons)
Strain
J
FUN_000880 Cadherin-like domain-containing protein
Strain 1 vs. Strain 2
Strain 1 vs. Strain 3
Strain 2 vs. Strain 3
Ka/Ks ratio
Position in base pair
extracellular
tm
cyt
Cadherin-like (IPR002126)
EGF-like domain (IPR000742)
I
Most enriched domains with KaKs >2 (Strain 1 versus Strain 2)
Cadherin-like
Protein kinase-like superfamily
WD40/YVTN repeat-like-containing
Armadillo-type fold
PDZ superfamily
Knr4/Smi1-like superfamily
Synembryn
Hedgehog protein, Hint domain
Protein patched/dispatched
TM protein family 132, middle dom.
-log10(p)
Count
J'
FUN_000880
# of non-synonymous substitutions
Strain
K
splash pool
evaporation
2X
aggregation
sheet expansion
(2)
refilling
clonal division
(1)
enhanced growth & feeding
swimmer cells
multicellularity favored
unicellularity favored
low salinity
1X
3X
high salinity
cyst-to-flagellate
(6)
(3)
sheet dissociation
survival from desiccation
cyst cells
(5)
single cells
(4)
cell death
desiccation
dry

780

781

Figure 6. *C. flexa* aggregation is constrained by kin recognition.
(A) Source location of the three distinct strains of *C. flexa* used in kin recognition experiments. (B) Aerial view of the M44 and M60 splash pools in the Exped-B site, from which Strains 2 and 3 were respectively isolated. Dashed lines: splash pool outlines. (C) Phylogenomic tree of Strains 1, 2 and 3, including single-sheet-bottleneck cultures (SSB) and three to four single-cell bottlenecked clones from each strain. (D) Cells of the same strain (here Strain 1), marked with magenta or green fluorophores, readily aggregated together regardless of colour, resulting in chimeric colonies (white arrowhead; compare **Figure 2H**). (E) Cells of Strains 1 and 3 (clone 1), marked with distinct fluorophores, readily aggregate into chimeric sheets (white arrowhead). (F) Cells of Strains 1 and 2 (clone 1), marked with distinct fluorophores, preferentially aggregate with their own strain, resulting in colonies with little or no chimerism (magenta and green arrowheads), indicating kin recognition. (G) Quantification of kin recognition using a segregation index (s) in different pairwise strain combinations (see **Figure S22** and Materials and Methods). The s index is calculated based on the proportion of green (or red) cells across sheets for a given combination of strains (as in[98]). An s index of 0 indicates no kin discrimination, while an s index of 1 indicates complete segregation of strains, and thus kin discrimination (**Figure S22B**, see Materials and Methods). p = 1.75e-09 by a one-way ANOVA. (H) Number of genes with high Ka/Ks regions (Ka/Ks > 2) for each pairwise comparison of strains. (I) Top 10 InterProScan domain annotations enriched in high Ka/Ks ratio regions in the Strain 1 versus Strain 2 comparison (p-value, Fisher's exact test). Domain IDs: Cadherin-like (IPR002126); Protein kinase-like domain superfamily (IPR011009); WD40/YVTN repeat-like-containing domain superfamily (IPR015943); Armadillo-type fold (IPR016024); PDZ superfamily (IPR036034); Knr4/Smi1-like domain superfamily (IPR037883); Synembryn (IPR008376); Hedgehog protein, Hint domain (IPR001767); Protein patched/dispatched (IPR003392); Transmembrane protein family 132, middle domain (IPR031437). (J) Top candidate kin recognition gene encoding a cadherin-like domain-containing protein (FUN_000880) with a potential role in cell-cell adhesion. Upper row: Ka/Ks ratio along the gene coding sequence in each pairwise strain combination (red: Strain 1 vs. Strain 2; blue: Strain 1 vs. Strain 3; green: Strain 2 vs. Strain 3). Lower row: InterProScan domain architecture schematics. Tm: transmembrane domain; cyt: cytoplasmic domain. (J') Number of non-synonymous substitutions in FUN_000880 for all pairwise strain combinations. (K) Summary schematic of *C. flexa* mixed clonal-aggregative multicellularity entrained by natural splash pool evaporation-refilling cycles. Multicellularity is favoured in low salinity, where sheets can form both by clonal division and by aggregation, and exhibit enhanced growth and prey capture (turquoise): (1) unicellular flagellate cells can divide clonally and/or aggregate to form multicellular sheets, maintaining direct cell-cell adhesions in their collar (magenta arrowheads); (2) sheets expand by clonal division, by aggregation of individual cells, and by sheet fusion. (3) Gradual evaporation leads to increase in salinity to medium-high levels, which prevents clonality but still allows aggregation and multicellularity. High salinity (>3-fold salinity) favours unicellularity (magenta): (4) *C. flexa* sheets dissociate into single cells that are incapable of proliferation and occasionally undergo cell death (5). Gradual evaporation, instead, results in the differentiation of flagellates into cysts (6) capable of surviving desiccation. (7) Rehydration restores permissive salinity and induces differentiation of cysts into flagellates, which can engage in clonal-aggregative multicellularity. Figure related to **Figures S20-S23, Table S3,** and **Supplementary Files S5-S6**.

825 # References

826 1. Grosberg, R. K. & Strathmann, R. R. The Evolution of Multicellularity: A Minor Major
827 Transition? *Annu. Rev. Ecol. Evol. Syst.* **38**, 621–654 (2007).
828 2. Sebé-Pedrós, A., Degnan, B. M. & Ruiz-Trillo, I. The origin of Metazoa: a unicellular
829 perspective. *Nat. Rev. Genet.* https://doi.org/10.1038/nrg.2017.21 (2017)
830 doi:10.1038/nrg.2017.21.
831 3. Bonner, J. T. The origins of multicellularity. *Integrative Biology* **1**, 27–36 (1998).
832 4. Brunet, T. & King, N. The Origin of Animal Multicellularity and Cell Differentiation.
833 *Dev. Cell* **43**, 124–140 (2017).
834 5. Staps, M., Van Gestel, J. & Tarnita, C. E. Emergence of diverse life cycles and life
835 histories at the origin of multicellularity. *Nat Ecol Evol* **3**, 1197–1205 (2019).
836 6. Márquez-Zacarías, P., Conlin, P. L., Tong, K., Pentz, J. T. & Ratcliff, W. C. Why have
837 aggregative multicellular organisms stayed simple? *Curr Genet* **67**, 871–876 (2021).
838 7. Schaap, P. Eukaryote Aggregative Multicellularity: Phylogenetic Distribution and a
839 Case Study of Its Proximate and Ultimate Cause in Dictyostelia. in *The Evolution of*
840 *Multicellularity* (CRC Press, 2022).
841 8. Leger, M. M. & Ruiz-Trillo, I. Phylogenetics of Clonal Multicellularity. in *The*
842 *Evolution of Multicellularity* (CRC Press, 2022).
843 9. Fisher, R. M., Cornwallis, C. K. & West, S. A. Group Formation, Relatedness, and the
844 Evolution of Multicellularity. *Current Biology* **23**, 1120–1125 (2013).
845 10. Kapsetakia, S. E., Tep, A. & West, S. A. How do algae form multicellular groups?
846 *Evolutionary Ecology Research* **18**, 663–675 (2017).
847 11. King, N. The unicellular ancestry of animal development. *Dev. Cell* **7**, 313–325 (2004).

848 12. Fairclough, S. R., Dayel, M. J. & King, N. Multicellular development in a
849 choanoflagellate. *Curr. Biol.* **20**, R875-876 (2010).
850 13. Leadbeater, B. S. C. *The Choanoflagellates: Evolution, Biology and Ecology*.
851 (Cambridge University Press, 2014).
852 14. Brunet, T. *et al.* Light-regulated collective contractility in a multicellular
853 choanoflagellate. *Science* **366**, 326–334 (2019).
854 15. Mehdiabadi, N. J., Kronforst, M. R., Queller, D. C. & Strassmann, J. E. Phylogeny,
855 reproductive isolation and kin recognition in the social amoeba Dictyostelium
856 purpureum. *Evolution* **63**, 542–548 (2009).
857 16. Ho, H.-I., Hirose, S., Kuspa, A. & Shaulsky, G. Kin recognition protects cooperators
858 against cheaters. *Curr Biol* **23**, 1590–1595 (2013).
859 17. Chaine, A. S., Schtickzelle, N., Polard, T., Huet, M. & Clobert, J. Kin-based recognition
860 and social aggregation in a ciliate. *Evolution* **64**, 1290–1300 (2010).
861 18. Benabentos, R. *et al.* Polymorphic members of the lag gene family mediate kin
862 discrimination in Dictyostelium. *Curr. Biol.* **19**, 567–572 (2009).
863 19. Lamża, Ł. Diversity of 'simple' multicellular eukaryotes: 45 independent cases and six
864 types of multicellularity. *Biological Reviews* **98**, 2188–2209 (2023).
865 20. Velicer, M. L. F., Kaitlin A. Schaal, Gregory J. Group Formation: On the Evolution of
866 Aggregative Multicellularity. in *The Evolution of Multicellularity* (CRC Press, 2022).
867 21. Ros-Rocher, N., Pérez-Posada, A., Leger, M. M. & Ruiz-Trillo, I. The origin of
868 animals: an ancestral reconstruction of the unicellular-to-multicellular transition. *Open*
869 *Biology* **11**, 200359 (2021).

870 22. Booth, D. S. & King, N. The history of Salpingoeca rosetta as a model for
871 reconstructing animal origins. in *Current Topics in Developmental Biology* vol. 147 73–
872 91 (Elsevier, 2022).
873 23. Ros-Rocher, N. & Brunet, T. What is it like to be a choanoflagellate? Sensation,
874 processing and behavior in the closest unicellular relatives of animals. *Anim Cogn* **26**,
875 1767–1782 (2023).
876 24. Carr, M., Leadbeater, B. S. C., Hassan, R., Nelson, M. & Baldauf, S. L. Molecular
877 phylogeny of choanoflagellates, the sister group to Metazoa. *Proc. Natl. Acad. Sci.*
878 *U.S.A.* **105**, 16641–16646 (2008).
879 25. Leadbeater, B. S. C. *The Choanoflagellates: Evolution, Biology and Ecology*.
880 (Cambridge University Press, Cambridge, 2015). doi:10.1017/CBO9781139051125.
881 26. Dayel, M. J. *et al.* Cell differentiation and morphogenesis in the colony-forming
882 choanoflagellate Salpingoeca rosetta. *Dev. Biol.* **357**, 73–82 (2011).
883 27. Ruiz-Trillo, I., Kin, K. & Casacuberta, E. The Origin of Metazoan Multicellularity: A
884 Potential Microbial Black Swan Event. *Annu. Rev. Microbiol.* **77**, 499–516 (2023).
885 28. Hehenberger, E. *et al.* Novel Predators Reshape Holozoan Phylogeny and Reveal the
886 Presence of a Two-Component Signaling System in the Ancestor of Animals. *Curr Biol*
887 **27**, 2043-2050.e6 (2017).
888 29. Sebé-Pedrós, A. *et al.* Regulated aggregative multicellularity in a close unicellular
889 relative of metazoa. *eLife* **2**, e01287 (2013).
890 30. Mylnikov, A. P., Tikhonenkov, D. V., Karpov, S. A. & Wylezich, C. Microscopical
891 Studies on *Ministeria vibrans* Tong, 1997 (Filasterea) Highlight the Cytoskeletal

892 Structure of the Common Ancestor of Filasterea, Metazoa and Choanoflagellata. *Protist*
893 **170**, 385–396 (2019).
894 31. Tikhonenkov, D. V. *et al.* New Lineage of Microbial Predators Adds Complexity to
895 Reconstructing the Evolutionary Origin of Animals. *Current Biology* **30**, 4500-4509.e5
896 (2020).
897 32. Dudin, O. *et al.* A unicellular relative of animals generates a layer of polarized cells by
898 actomyosin-dependent cellularization. *eLife* **8**, e49801 (2019).
899 33. Shah, H. *et al.* Life-cycle-coupled evolution of mitosis in close relatives of animals.
900 *Nature* **630**, 116–122 (2024).
901 34. Olivetta, M., Bhickta, C., Chiaruttini, N., Burns, J. & Dudin, O. A multicellular
902 developmental program in a close animal relative. Preprint at
903 https://doi.org/10.1101/2024.03.25.586530 (2024).
904 35. Shabardina, V. *et al.* Ichthyosporea: a window into the origin of animals. *Commun Biol*
905 **7**, 915 (2024).
906 36. Marshall, W. L. & Berbee, M. L. Facing Unknowns: Living Cultures (Pirum gemmata
907 gen. nov., sp. nov., and Abeoforma whisleri, gen. nov., sp. nov.) from Invertebrate
908 Digestive Tracts Represent an Undescribed Clade within the Unicellular Opisthokont
909 Lineage Ichthyosporea (Mesomycetozoea). *Protist* **162**, 33–57 (2011).
910 37. Brunet, T. *et al.* Light-regulated collective contractility in a multicellular
911 choanoflagellate. *Science* **366**, 326–334 (2019).
912 38. Reyes-Rivera, J. *et al.* Nitric oxide signaling controls collective contractions in a
913 colonial choanoflagellate. *Current Biology* **32**, 2539-2547.e5 (2022).

914 39. Fairclough, S. R., Dayel, M. J. & King, N. Multicellular development in a
915 choanoflagellate. *Current Biology* **20**, R875–R876 (2010).
916 40. Keller, E. F. & Segel, L. A. Initiation of slime mold aggregation viewed as an
917 instability. *Journal of Theoretical Biology* **26**, 399–415 (1970).
918 41. Leadbeater, B. S. Life-history and ultrastructure of a new marine species of
919 Proterospongia (Choanoflagellida). *Journal of the Marine Biological Association of the*
920 *United Kingdom* **63**, 135–160 (1983).
921 42. Little, C. & Kitching, J. A. *The Biology of Rocky Shores*. (Oxford University Press,
922 1996).
923 43. Garbary, D. The Margin of the Sea. in *Algae and Cyanobacteria in Extreme*
924 *Environments* (ed. Seckbach, J.) 173–191 (Springer Netherlands, Dordrecht, 2007).
925 doi:10.1007/978-1-4020-6112-7_9.
926 44. Huggett, J. & Griffiths, C. Some relationships between elevation, physico-chemical
927 variables and biota of intertidal rock pools. *Mar. Ecol. Prog. Ser.* **29**, 189–197 (1986).
928 45. Amsalem, E. & Rilov, G. High thermal plasticity, and vulnerability, in extreme
929 environments at the warm distributional edge: The case of a tidepool shrimp. *Journal of*
930 *Experimental Marine Biology and Ecology* **545**, 151641 (2021).
931 46. Davison, I. R. & Pearson, G. A. Stress Tolerance in Intertidal Seaweeds. *Journal of*
932 *Phycology* **32**, 197–211 (1996).
933 47. Leadbeater, B. S. C. & Karpov, S. A. Cyst Formation in a Freshwater Strain of the
934 Choanoflagellate Desmarella moniliformis Kent. *Journal of Eukaryotic Microbiology*
935 **47**, 433–439 (2000).

936 48. Stoupin, D. *et al.* Cryptic diversity within the choanoflagellate morphospecies complex
937 *Codosiga botrytis* – Phylogeny and morphology of ancient and modern isolates.
938 *European Journal of Protistology* **48**, 263–273 (2012).
939 49. Jeuck, A., Arndt, H. & Nitsche, F. Extended phylogeny of the Craspedida
940 (Choanomonada). *European Journal of Protistology* **50**, 430–443 (2014).
941 50. Li, Y., Wang, Y., Zhang, S., Maurer-Alcalá, X. X. & Yan, Y. How Ciliated Protists
942 Survive by Cysts: Some Key Points During Encystment and Excystment. *Frontiers in*
943 *Microbiology* **13**, (2022).
944 51. Schaap, P. & Schilde, C. Encystation: the most prevalent and underinvestigated
945 differentiation pathway of eukaryotes. *Microbiology* **164**, 727–739 (2018).
946 52. Verni, F. & Rosati, G. Resting cysts: A survival strategy in Protozoa Ciliophora. *Italian*
947 *Journal of Zoology* **78**, 134–145 (2011).
948 53. Di Ciano, C. *et al.* Osmotic stress-induced remodeling of the cortical cytoskeleton.
949 *American Journal of Physiology-Cell Physiology* **283**, C850–C865 (2002).
950 54. Komis, G., Apostolakos, P. & Galatis, B. Hyperosmotic stress-induced actin filament
951 reorganization in leaf cells of Chlorophyton comosum. *Journal of Experimental Botany*
952 **53**, 1699–1710 (2002).
953 55. Rivero, F. *et al.* The role of the cortical cytoskeleton: F-actin crosslinking proteins
954 protect against osmotic stress, ensure cell size, cell shape and motility, and contribute to
955 phagocytosis and development. *Journal of Cell Science* **109**, 2679–2691 (1996).
956 56. Aizawa, H. *et al.* Hyperosmotic stress-induced reorganization of actin bundles in
957 Dictyostelium cells over-expressing cofilin. *Genes to Cells* **4**, 311–324 (1999).

958 57. Bonner, J. T. Aggregation and Differentiation in the Cellular Slime Molds. *Annual*
959 *Review of Microbiology* **25**, 75–92 (1971).
960 58. Balachandra, S., Sarkar, S. & Amodeo, A. A. The Nuclear-to-Cytoplasmic Ratio:
961 Coupling DNA Content to Cell Size, Cell Cycle, and Biosynthetic Capacity. *Annu Rev*
962 *Genet* **56**, 165–185 (2022).
963 59. Griffiths, A. J. Encystment in Amoebae. in *Advances in Microbial Physiology* (eds
964 Rose, A. H. & Wilkinson, J. F.) vol. 4 105–129 (Academic Press, 1969).
965 60. Fenchel, T. Filter-feeding in Colonial Protists. *Protist* **170**, 283–286 (2019).
966 61. Koehl, M. a. R. Selective factors in the evolution of multicellularity in
967 choanoflagellates. *Journal of Experimental Zoology Part B: Molecular and*
968 *Developmental Evolution* **336**, 315–326 (2021).
969 62. Cavalier-Smith, T. Origin of animal multicellularity: precursors, causes,
970 consequences—the choanoflagellate/sponge transition, neurogenesis and the Cambrian
971 explosion. *Philosophical Transactions of the Royal Society B: Biological Sciences* **372**,
972 20150476 (2017).
973 63. Kirkegaard, J. B. & Goldstein, R. E. Filter-feeding, near-field flows, and the
974 morphologies of colonial choanoflagellates. *Phys. Rev. E* **94**, 052401 (2016).
975 64. L'Etoile, N. J. & King-Smith, C. Rosette Colonies of Choanoflagellates (Salpingoeca
976 rosetta) Show Increased Food Vacuole Formation Compared with Single Swimming
977 Cells. *Journal of Eukaryotic Microbiology* **67**, 263–267 (2020).
978 65. Sternfeld, J. Evidence for differential cellular adhesion as the mechanism of sorting-out
979 of various cellular slime mold species. *J Embryol Exp Morphol* **53**, 163–178 (1979).

980 66. Wolpert, L. & Szathmáry, E. Multicellularity: Evolution and the egg. *Nature* **420**, 745–
981 745 (2002).
982 67. King, N. *et al.* The genome of the choanoflagellate Monosiga brevicollis and the origin
983 of metazoans. *Nature* **451**, 783–788 (2008).
984 68. Fairclough, S. R. *et al.* Premetazoan genome evolution and the regulation of cell
985 differentiation in the choanoflagellate Salpingoeca rosetta. *Genome Biol* **14**, R15
986 (2013).
987 69. Hirose, S., Benabentos, R., Ho, H.-I., Kuspa, A. & Shaulsky, G. Self-recognition in
988 social amoebae is mediated by allelic pairs of tiger genes. *Science* **333**, 467–470 (2011).
989 70. Tarnita, C. E., Taubes, C. H. & Nowak, M. A. Evolutionary construction by staying
990 together and coming together. *Journal of Theoretical Biology* **320**, 10–22 (2013).
991 71. Tang, S., Pichugin, Y. & Hammerschmidt, K. An environmentally induced multicellular
992 life cycle of a unicellular cyanobacterium. *Current Biology* **33**, 764-769.e5 (2023).
993 72. Mizuno, K. *et al.* Novel multicellular prokaryote discovered next to an underground
994 stream. *eLife* **11**, e71920 (2022).
995 73. Barrere, J., Nanda, P. & Murray, A. W. Alternating selection for dispersal and
996 multicellularity favors regulated life cycles. *Current Biology* **33**, 1809-1817.e3 (2023).
997 74. Pichugin, Y., Park, H. J. & Traulsen, A. Evolution of simple multicellular life cycles in
998 dynamic environments. *J. R. Soc. Interface.* **16**, 20190054 (2019).
999 75. Staps, M., Van Gestel, J. & Tarnita, C. E. Life Cycles as a Central Organizing Theme
1000 for Studying Multicellularity. in *The Evolution of Multicellularity* (CRC Press, 2022).
1001 76. H. James-Clark A. B. IV.—Conclusive proofs of the animality of the ciliate sponges,
1002 and of their affinities with the Infusoria flagellata. *Annals and Magazine of Natural*

1003 *History* https://doi.org/10.1080/00222936708679703 (1867)
1004 doi:10.1080/00222936708679703.
1005 77. Hibberd, D. J. Observations on the ultrastructure of the choanoflagellate Codosiga
1006 botrytis (Ehr.) saville-kent with special reference to the flagellar apparatus. *Journal of*
1007 *Cell Science* **17**, 191–219 (1975).
1008 78. Pettitt, M. E., Orme, B. A. A., Blake, J. R. & Leadbeater, B. S. C. The hydrodynamics
1009 of filter feeding in choanoflagellates. *European Journal of Protistology* **38**, 313 (2002).
1010 79. Brunet, T. & King, N. The Origin of Animal Multicellularity and Cell Differentiation.
1011 *Developmental Cell* **43**, 124–140 (2017).
1012 80. Nagy, L. G., Varga, T., Csernetics, Á. & Virágh, M. Fungi took a unique evolutionary
1013 route to multicellularity: Seven key challenges for fungal multicellular life. *Fungal*
1014 *Biology Reviews* **34**, 151–169 (2020).
1015 81. Brown, M. W., Spiegel, F. W. & Silberman, J. D. Phylogeny of the 'forgotten' cellular
1016 slime mold, Fonticula alba, reveals a key evolutionary branch within Opisthokonta. *Mol*
1017 *Biol Evol* **26**, 2699–2709 (2009).
1018 82. Toret, C., Picco, A., Boiero-Sanders, M., Michelot, A. & Kaksonen, M. The cellular
1019 slime mold *Fonticula alba* forms a dynamic, multicellular collective while feeding on
1020 bacteria. *Current Biology* **32**, 1961-1973.e4 (2022).
1021 83. Sauer, K. *et al.* The biofilm life cycle: expanding the conceptual model of biofilm
1022 formation. *Nat Rev Microbiol* **20**, 608–620 (2022).
1023 84. Chavhan, Y., Dey, S. & Lind, P. A. Bacteria evolve macroscopic multicellularity by the
1024 genetic assimilation of phenotypically plastic cell clustering. *Nat Commun* **14**, 3555
1025 (2023).

1026 85. Pentz, J. T. *et al.* Evolutionary consequences of nascent multicellular life cycles. *eLife*
1027 **12**, e84336 (2023).
1028 86. Rose, C. J. & Hammerschmidt, K. What Do We Mean by Multicellularity? The
1029 Evolutionary Transitions Framework Provides Answers. *Front. Ecol. Evol.* **9**, 730714
1030 (2021).
1031 87. Pentz, J. T. *et al.* Evolutionary consequences of nascent multicellular life cycles. *eLife*
1032 **12**, e84336 (2023).
1033 88. Hammerschmidt, K., Rose, C. J., Kerr, B. & Rainey, P. B. Life cycles, fitness
1034 decoupling and the evolution of multicellularity. *Nature* **515**, 75–79 (2014).
1035 89. Michod, R. E. Evolution of individuality during the transition from unicellular to
1036 multicellular life. *Proc. Natl. Acad. Sci. U.S.A.* **104 Suppl 1**, 8613–8618 (2007).
1037 90. Jahan, I., Scott, T. J., Strassmann, J. E. & Queller, D. C. Testing the coordination
1038 hypothesis: incompatibilities in aggregative development of an experimentally evolved
1039 social amoeba. *Evolution Letters* **9**, 236–248 (2025).
1040 91. Smith, J., Strassmann, J. E. & Queller, D. C. Fine-scale spatial ecology drives kin
1041 selection relatedness among cooperating amoebae. *Evolution* **70**, 848–859 (2016).
1042 92. West, S. A., Griffin, A. S. & Gardner, A. Social semantics: altruism, cooperation,
1043 mutualism, strong reciprocity and group selection. *J of Evolutionary Biology* **20**, 415–
1044 432 (2007).
1045 93. Haag, C. R., Riek, M., Hottinger, J. W., Pajunen, V. I. & Ebert, D. Founder events as
1046 determinants of within-island and among-island genetic structure of Daphnia
1047 metapopulations. *Heredity* **96**, 150–158 (2006).

1048 94. Black, A. J., Bourrat, P. & Rainey, P. B. Ecological scaffolding and the evolution of
1049 individuality. *Nat Ecol Evol* **4**, 426–436 (2020).
1050 95. Brunet, T. & King, N. The Single-Celled Ancestors of Animals: A History of
1051 Hypotheses. in *The evolution of multicellularity* (CRC Press, 2022).
1052 96. Ferrer-Bonet, M. & Ruiz-Trillo, I. Capsaspora owczarzaki. *Current Biology* **27**, R829–
1053 R830 (2017).
1054 97. Grau-Bové, X. *et al.* Dynamics of genomic innovation in the unicellular ancestry of
1055 animals. *Elife* **6**, (2017).
1056 98. Estrela, S. & Brown, S. P. Metabolic and Demographic Feedbacks Shape the Emergent
1057 Spatial Structure and Function of Microbial Communities. *PLoS Comput Biol* **9**,
1058 e1003398 (2013).
1059